Engineering Fracture Mechanics 281 (2023) 109048

Contents lists available at ScienceDirect

Engineering Fracture Mechanics

journal homepage: www.elsevier.com/locate/engfracmech

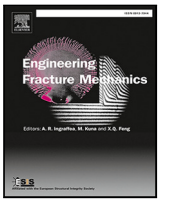

Endowing Griffith's fracture theory with the ability to describe fatigue cracks

Roberto Alessi [a,*], Jacinto Ulloa [b]

[a] Department of Civil and Industrial Engineering, University of Pisa, Largo Lucio Lazzarino 2, 56122, Pisa, Italy
[b] Division of Engineering and Applied Science, California Institute of Technology, 1200 E. California Blvd., Pasadena, CA 91125, USA

ARTICLE INFO

Keywords:
Fatigue
Griffith's fracture theory
History variable
State-dependent fracture toughness
Paris' law

ABSTRACT

In this paper, a possible extension of Griffith's fracture theory to describe fatigue-induced crack propagation is proposed. To this end, an energy-based model is presented, taking Griffith's model as the point of departure and employing the concept of state-dependent fracture toughness. Therein, fatigue degradation is achieved through a suitable history variable endowed with a functional form that is able to consider crucial aspects of fatigue, including the crack-tip singularity, the identification of fatigue-inducing loading conditions, and mean load effects. Simple paradigmatic examples indicate that the model provides a unified description of different fatigue responses and unveils peculiar regimes in the crack propagation process, always preserving the link to classical fracture mechanics. In this context, analytical results establish a clear relation between Griffith's fracture theory and Paris' law. The proposed modeling framework paves the way for future developments in modern fracture mechanics, *e.g.*, to derive a novel generation of variational fatigue phase-field fracture models suitably rooted in a Griffith-based theory.

1. Introduction

Fatigue refers to a failure process due to the application of repeated loads, which individually would be too small to cause the direct failure of the material itself. As a consequence of such repeated loadings (cyclic or not), various complex interacting phenomena occur at the micro-scale, having almost all in common the weakening and degradation of the material properties at the macro-scale. Such microscopic phenomena consist, for instance, of plastic slip systems and the coalescence of micro-voids [1–3]. As the fatigue process advances, these microdefects, which are ruled by the stochastic micro-structural arrangement of the material and therefore are random in nature, evolve into microcracks. The resulting microcracks eventually coalesce and lead to the formation of a fatigue (macro-)crack, whose size allows one to neglect the aleatory nature of the material microstructure. This macro-crack may then propagate, first in a stable way, and finally unstably leading to failure.

Fatigue failure is an extremely, if not the most, dangerous phenomenon in structural mechanics, since it often occurs without forewarning resulting in devastating events. Precisely, it is responsible for up to 90% of all mechanical failures and involves the majority of materials [4]. Moreover, in real situations, the identification of the fatigue degradation state of a material is very difficult if not impossible. Therefore, fatigue failure prediction still represents an open challenge for modeling and simulation at the cutting edge of mechanics.

Fracture mechanics is nowadays a consolidated theory within the realm of continuum mechanics that has been developed starting from the pioneering work of Griffith [5], where the key concepts of energy release rate and fracture toughness were established. A

* Corresponding author.
E-mail addresses: roberto.alessi@unipi.it (R. Alessi), julloa@caltech.edu (J. Ulloa).

https://doi.org/10.1016/j.engfracmech.2023.109048
Received 25 October 2022; Received in revised form 17 December 2022; Accepted 1 January 2023
Available online 13 January 2023

Nomenclature

Acronyms

FDZ	fatigue degradation zone
FR	fast crack propagation regime
HCF	high-cycle fatigue
KPZ	K-dominance zone
LEFM	linear elastic fracture mechanics
PR	Paris' (stable) crack propagation regime
SR	slow crack propagation regime

Standard mechanical symbols

(ρ, ϑ)	crack tip polar coordinates
$\mathcal{D}$	dissipation potential
ψ	elastic energy density
$\mathcal{P}$	total potential energy
ν	Poisson's ratio
σ	far field stress
$\boldsymbol{x}$	generic position vector
E	Young's modulus
t	time-evolution parameter

Fracture related symbols

$\bar{\Lambda}$	K-dominance degree limit
Γ	crack path domain ($\Gamma = \hat{\Gamma} \cup \check{\Gamma}$ and $\hat{\Gamma} \cap \check{\Gamma} = \emptyset$)
$\check{\Gamma}$	sound part of the crack path
$\hat{\Gamma}$	current open crack
G_{c}	fracture toughness
$\hat{\boldsymbol{x}}$	crack position vector map
K_{Ic}	mode-I critical stress intensity factor
Λ_{ψ}	energy based K-dominance degree
Λ_{σ}	stress based K-dominance degree
l	current crack length
l_0	initial crack length
r	relative crack arc-length ($r = s - l$)
s	crack arc-length
$\boldsymbol{x}_l$	crack tip position vector
$\boldsymbol{r}$	relative crack tip position vector
G	energy release rate
K_i	mode-i stress intensity factor

Fatigue related symbols

$\mathcal{D}_{\mathrm{f}}$	fatigue dissipation potential
$\bar{\psi}$	elastic energy based fatigue history variable
d	fatigue degradation function
f	fatigue function
ϕ	fatigue history variable
ϕ_0	fatigue history variable at critical monotonic load
G_{f}	fatigue fracture toughness
k_{f}	fatigue degradation parameter
k_{h}	fatigue threshold function parameter

remarkable variational extension of such a theory was proposed by Francfort and Marigo [6], where the quasistatic crack evolution was revisited as an energy minimization problem and freed from the usual Griffith's constraints, namely, the existence of a preexisting crack and a well defined crack path. Along its merits, one cannot avoid mentioning the effective numerical phase-field approach [7]

ℓ_f	fatigue length
ℓ_k	K-dominance length
C	Paris' (law) coefficient
h	fatigue threshold function
m	Paris' (law) exponent
N	cycle number
R	fatigue load ratio

built on the top on this variational framework by [8] which has made possible the simulation and prediction of very complex fracture phenomena.

This work aims at contributing to the development of a new generation of phase-field models endowed with the capability of describing both fatigue crack initiation (*e.g.* Wöheler limits) and fatigue crack propagation (*e.g.* Paris' law). In this regard, recent and promising attempts have been made so far. These can be divided with respect to the modeling strategy adopted for taking into account fatigue effects. Under the thermodynamical point of view, the first main difference is whether fatigue effects are assumed increasing the damage/fracture driving force or reducing the damage/fracture resisting force. To the former class belong, for instance, Refs. [9–11]. In these works, an additional energetic source is introduced, which depends on a dedicated fatigue variable whose evolution is governed by a cyclic-number dependent law. Among the models that consider fatigue effects as a reduction of the resisting force, different modeling strategies have been considered. In [12], in the context of a one-dimensional energetic formulation framework [13], the fracture toughness is reduced by means of a history variable. Existence results of this model have been investigated with a vanishing viscosity approach [14]. A three-dimensional extension of this model was provided in [15] and an efficient numerical implementation in [16]. This model has been extended in [17–19] to consider plasticity effects, therefore capturing ductile fatigue fracture phenomena, and in [20] in a multi-physics context for modeling fatigue cracking in lithium-ion battery electrode particles. In [21–23], an additional fatigue damage variable has been introduced and its evolution law directly prescribed, that is, not descending from the variational framework. Such an auxiliary variable reduces the fracture toughness by means of a degradation function. Within the same approach, polymeric materials have been considered in a finite strains setting in [24]. Other models, which cannot be categorized in the two above mentioned classes, directly modify or enrich the phase-field evolution law. For instance, in [25], a phase-field viscosity fatigue effect is considered. In [26], fatigue effects have been taken into account by degrading with respect to damage the stress appearing in the Ginzburg–Landau (G–L) equation. In [27,28], fatigue is modeled as a continuous internal variable whose evolution equation is considered as a constitutive relation to be determined in a thermodynamically consistent way. Similarly, [29] considers fatigue effects in elasto-plastic solids and in a non-isothermal setting. Fatigue effects in a viscous-elastic material are considered in [30–32] by adding a phenomenological damage rate dependent energetic term in the balance of mechanical energy.

Despite the interesting insights and results, none of the previously mentioned models has proven to own the required flexibility and, at the same time, to be sufficiently simple in describing real material fatigue behaviors. The main reason, in our opinion, lies in the fact that all these models have been derived directly from phase-field models and not as regularization of a Griffith's type fracture model able to describe fatigue effects. Therefore, in view of the above mentioned long term goal, the main aim of this work is to establish a first link, in our opinion necessary, between Griffith's fracture theory and Paris-like fatigue crack propagation laws for the description of high-cycle fatigue (HCF) phenomena. To the authors' knowledge, such a link has not been established yet.

In this regard, the proposed model will be shown, for instance, to be sufficiently flexible to describe several key features of fatigue crack propagation, like the Paris' law regime, the vertical asymptotic monotonic fracture limit, and mean stress effects. We will also show how all these features, that we believe any model should be able to describe in a unified manner, can be easily tuned.

The key idea of the present model, inspired by Alessi et al. [12], is to no longer consider the fracture toughness as a material parameter but rather as a material function. Specifically, the fracture toughness is assumed to decrease as an accumulated *fatigue variable*, an energy-based measure in this work, increases. We will call the fatigue variable accumulation *fatigue history variable*. Moreover, a fatigue zone surrounding the crack tip is introduced in order to amplify the fatigue degradation effects. The energy amplification in this region is motivated by the fact that in HCF problems, even involving ductile materials, inelastic phenomena strongly influencing the fatigue crack growth rate only occur around the crack tip. This modeling approach amounts to a phenomenological description of a multitude of microscopic material degradation mechanisms.

Due to the novelty of the model, the presentation is kept at its maximum level of simplicity, leaving deeper investigations and refinements to future works. Therefore, only a two-dimensional problem is considered with a single evolving crack and mode-I loading conditions. Nevertheless, many other problems can be immediately considered taking advantage of the results presented in fracture mechanics handbooks, as, for instance, in [33].

The remainder of the paper is structured as follows. Section 2 presents, step by step, the construction of the proposed fatigue model, starting from Griffith's fracture governing equations. Key concepts such as the fatigue degradation zone, the fatigue degradation function, and the fatigue history variable are here introduced. In Section 3, a simple illustrative example highlighting the essential model features is presented. Therein, a closed-form link between the stationary fatigue crack propagation regime of the model and Paris' law is also established. Concluding remarks are finally drawn in Section 4 where future possible modeling extensions are discussed.

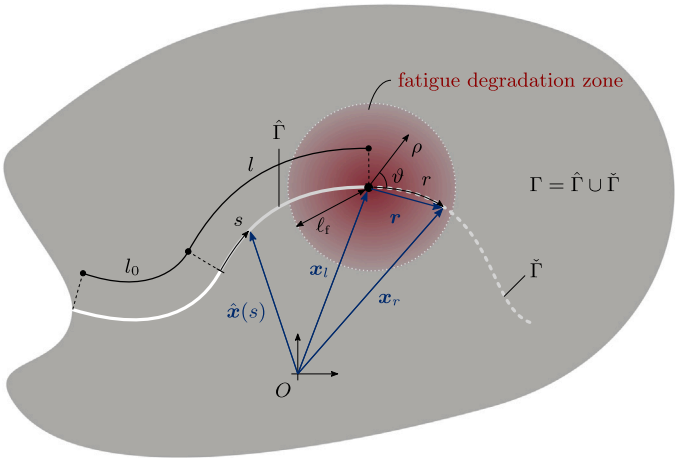

Fig. 1. Abstract problem setup.

Notation. ${}^t\square = \{\square(\tau) : \tau \in [0,t]\}$ identifies a history variable, $\dot{\square}$ or $(\square)^{\cdot}$ defines the total derivative with respect to time t, and $(\square)^+$ is the positive part of $\square$. Furthermore, we often name functions expressing the same physical quantity but depending on different variables, of course linked to each other, with the same label, when no source of confusion occurs. Similarly, the difference between a function and its value computed at a given state is not always made explicit.

2. From Griffith's fracture theory to a brittle fracture fatigue model

A two-dimensional mechanical problem is considered, with a homogeneous isotropic linear elastic material and a single, possibly non-straight, smooth crack. The crack path is arbitrary in the following abstract formulation, whereas in the forthcoming examples, a predefined crack path will be assumed in order to obtain analytical results. Mode-I loading conditions are considered. The evolution problem is assumed rate-independent and described by the time-evolution parameter t with initial conditions set up at $t = 0$. The *linear elastic fracture mechanics* (LEFM) framework is assumed, with a fracture process zone well smaller than the *K-dominance zone* (KDZ).

According to Fig. 1, the crack path Γ is parametrized by its arc-length s, that is, $s \mapsto \hat{\boldsymbol{x}}(s)$. The actual crack tip is identified by the crack length l with $\boldsymbol{x}_l = \hat{\boldsymbol{x}}(l)$, while r denotes the crack path arc-length with respect to the crack tip and $\boldsymbol{x}_r = \hat{\boldsymbol{x}}(l+r)$ the related position vector. The current crack is then denoted by $\hat{\Gamma}$ while its complement, the still unbroken crack, by $\check{\Gamma}$, such that $\Gamma = \hat{\Gamma} \cup \check{\Gamma}$.

In this work, we also introduce the concept of *fatigue degradation zone* (FDZ), that is, the region where the fatigue degradation process occurs. Often, as in [34], the FDZ is simply referred to as the region, formed within the plastic zone, in which the micro- or macroplastic cyclic strain takes place and the initial damage of the material microstructure originates [35]. For the purposes of this work, it is sufficient to consider the FDZ delimited by a circle centered at the crack tip and with radius denoted by ℓ_f. The *fatigue length* ℓ_f can then be regarded as a material internal length. Other shapes for the FDZ can be considered, as the one in [36, Fig. A.18] based on the elastic energy density field.

In the following sections, standard brittle and fatigue fracture mechanics results, respectively presented in Section 2.1 and Section 2.2, are first summarized. This summary serves as motivation and sets the stage for the *step-by-step* construction of the proposed fatigue model in Section 2.3. Specific expressions for the introduced fatigue material functions are proposed in Section 2.4.

2.1. Griffith's theory of fracture

In the present setting, Griffith's theory describing the evolution of a crack is based on the following conditions:

$$\begin{cases} G \le G_c, & \text{(a)} \\ \dot{l} \ge 0, & \text{(b)} \\ (G - G_c)\,\dot{l} = 0, & \text{(c)} \end{cases} \tag{1}$$

that must hold at any time t, with

$$G := -\frac{\partial \mathcal{P}}{\partial l} \tag{2}$$

being the *energy release rate*, depending on the *total potential energy* $\mathcal{P}$, sum of the total elastic potential energy and the work of external actions, and G_c the material *fracture toughness* [5,8]. Conditions (1) are also known as *Griffith's criterion*. From a thermodynamical viewpoint and interpreting the crack length as a global dissipating internal variable, the first condition (1a) compares the crack length driving force G to the resisting force G_c. Instead, conditions (1b) and (1c) enforce the fulfillment of

the Clausius–Duhem inequality (irreversibility condition) and energy balance, respectively. In the framework of *generalized standard materials* (GSM) [37], the problem (1) reduces to the following condition:

$$-\frac{\partial \mathcal{P}}{\partial l} \in \partial D\left(\dot{l}\right) \tag{3}$$

at any time t, with

$$D\left(\dot{l}\right) := \begin{cases} G_c\,\dot{l}, & \text{if } \dot{l} \geq 0, \\ +\infty, & \text{if } \dot{l} < 0, \end{cases} \tag{4}$$

being the (convex) dissipation potential satisfying $D(0) = 0$. An extensive discussion on the link between the two formulations can be found in [8, Sec. 2.1].

2.1.1. Stress intensity factors and the K-dominance zone

For two dimensional problems, the stress field near the crack tip of a linear elastic isotropic solid has a universal form independent of applied loads and the geometry of the cracked body [38], namely,

$$\sigma_{ij} = \underbrace{\frac{1}{\sqrt{2\pi\rho}}\left(K_{\mathrm{I}} f_{ij}^{\mathrm{I}}(\vartheta) + K_{\mathrm{II}} f_{ij}^{\mathrm{II}}(\vartheta) + K_{\mathrm{III}} f_{ij}^{\mathrm{III}}(\vartheta)\right)}_{\sigma_{ij}^{\mathrm{sing}}} + \underbrace{o\left(1/\sqrt{\rho}\right)}_{\sigma_{ij}^{\mathrm{reg}}}, \tag{5}$$

where $\sigma_{ij}^{\mathrm{sing}}$ and $\sigma_{ij}^{\mathrm{reg}}$ are, respectively, the *singular* and *regular* parts of the corresponding stress component σ_{ij} and (ρ, ϑ) are the local polar coordinates centered at the crack tip with respect to the tangent direction to the crack path. Consequently, the elastic energy density can also be approximated near the crack tip by its singular and regular parts:

$$\psi = \underbrace{\frac{1}{\rho}\,\kappa_\psi(\vartheta)}_{\psi^{\mathrm{sing}}} + \underbrace{o\left(1/\rho\right)}_{\psi^{\mathrm{reg}}}. \tag{6}$$

These representations of the stress and elastic energy density fields continue to be locally valid in case of a two-dimensional crack front in a three-dimensional body, with the only difference that the stress intensity factors and k_ψ also depend on the arc-length parametrization of the crack front and provided that the crack front has no special singular points, as for instance a kink of the crack front or a point where the crack front intersects a free surface. In such cases, the stress and the energy singularities are no longer of type $\rho^{-1/2}$ and ρ^{-1}, respectively [39, Sec. 4.2.3].

It is clear from (5) and (6) that singular parts become dominant in locations close to the crack tip. Indeed, in the KDZ, the near-tip stress field can be effectively described by the singular stress field or, equivalently, by the stress intensity factors.

For a mode-I fracture, the link between the energy release rate and the corresponding stress intensity factor yields

$$G = k_{\mathrm{G}} K_{\mathrm{I}}^2, \tag{7}$$

with $k_{\mathrm{G}} = 1/E$ for *plane-stress* and $k_{\mathrm{G}} = (1-\nu^2)/E$ for *plane-strain* elasticity. The link for the other fracture modes, including mixed ones, can be found in [38,40]. For mode-I fractures, (7) allows us to express Griffith's fracture criterion (1a) with respect to the stress intensity factor instead of the fracture toughness:

$$K_{\mathrm{I}} \leq K_{\mathrm{Ic}}, \quad \text{with} \quad K_{\mathrm{Ic}} := \sqrt{G_c/k_{\mathrm{G}}} \tag{8}$$

being the critical stress intensity factor.

The definition of the KDZ size is not unique and often depends on the specific problem. For instance, this region depends on the crack path geometry, including the crack length, the fracture mode, and a tolerance parameter which fixes the K-dominance degree. The K-dominance degree Λ is defined as the ratio between a singular part and the sum of the singular and regular parts of a component of the elastic solution. A value of Λ close to unity means that the singular part of the elastic solution is dominant. On the contrary, a value close to zero corresponds to a solution influenced only by the regular part.

Let us consider a mode-I fracture problem with a straight crack ($\rho = r$). Following the definition in [38, p. 66], we have that

$$\Lambda_\sigma(r) = \frac{\sigma_{\mathrm{sing}}(r)}{\sigma(r)}, \tag{9}$$

with $\sigma_{\mathrm{sing}}(r) = K_{\mathrm{I}}/\sqrt{2\pi r}$. The two stress values refer to the stress component $\sigma_{rr}(r, \vartheta = 0)$. A similar definition in terms of the elastic energy density can be provided:

$$\Lambda_\psi(r) = \frac{\psi_{\mathrm{sing}}(r)}{\psi(r)}. \tag{10}$$

Then, once a limit value for the K-dominance degree has been set, say $\bar{\Lambda}$, the K-dominance characteristic size ℓ_{k}, hereafter called *K-dominance length*, is given by

$$\ell_{\mathrm{k}} \,:\, \Lambda(\ell_{\mathrm{k}}) = \bar{\Lambda}, \tag{11}$$

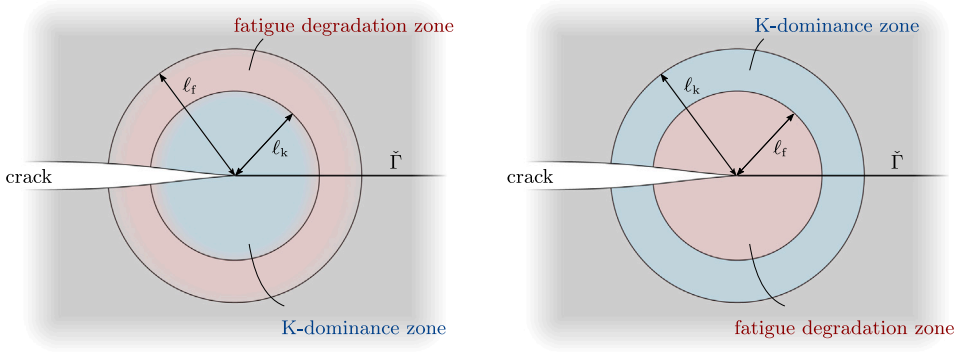

(a) $\ell_k < \ell_f$ (b) $\ell_k > \ell_f$

Fig. 2. K-dominance (blue) and fatigue degradation (red) zones.

with Λ equal to Λ_σ or Λ_ψ.

So far, three important regions around the crack tip have been introduced, namely, the fracture process zone, the K-dominance zone and the fatigue degradation zone. In this work and in agreement with the LEFM framework, both the K-dominance and the fatigue degradation zones are assumed to contain the fracture process zones whereas both situations where the fatigue degradation zone contains or is contained in the K-dominance zone will be considered (Fig. 2(a) and Fig. 2(b) respectively).

In special situations, (7) together with (1a) have been proven to be no longer valid, as for instance when the crack approaches a rigid boundary [41,42]. In this case, the fracture criterion must also account for the regular part of the elastic solution. This is usually accomplished by considering the fracture toughness not a pure material constant anymore. The eventuality of a non-constant fracture toughness is discussed in the next section and paves the way for the forthcoming fatigue model.

2.1.2. *Fracture toughness as a material function*

This section highlights situations where the fracture toughness cannot be considered a material parameter anymore but rather a material function. This will motivate and justify the introduction of a state-dependent fracture toughness, the key ingredient for capturing fatigue effects in the proposed fatigue model. Specifically, we believe worth mentioning the following cases:

i. *Fracture mode dependent fracture toughness*. The fracture mode itself may also influence the fracture criterion. As observed in [43], the fracture toughness for a mode-I crack may be significantly higher than the fracture toughness for a mode-II crack. However, in rocks, the opposite situation may occur [44]. In general, one has $G_c = G_c(\text{fracture mode})$.
ii. *Rate-dependent fracture toughness*. Many materials, such as polymers, are much more brittle when the loading rate is increased, exhibiting therefore a loading rate fracture toughness dependence [45, Sec. 5.2] and [46].
iii. *Environment dependent fracture toughness*. For instance, materials exposed to hydrogen may experience a very significant reduction in fracture toughness. This feature has been incorporated in brittle and cohesive fracture models [47,48] and in phase-field fracture models [49].
iv. *Non-homogeneous materials*. Non-homogeneous materials may exhibit a fracture toughness highly variable in space, that is a fracture toughness dependent on the material point. This is the case, for instance, of functionally graded materials (FGMs) [50,51].
v. *Crack-length and geometry dependent fracture toughness*. In some cases, the fracture toughness is not a material constant but rather an increasing function with respect to the crack propagation length, namely, $G_c = R(l)$ with $R'(l) \geq 0$. The function $R(l)$ is known as *crack growth resistance curve* and allows one to investigate stable crack propagation conditions. Usually, after a relatively short crack extension, an asymptotic value is reached and the fracture toughness remains constant for further crack advancements. The reasons for this toughening phenomenon are manifold. For instance, in metals, this is often due to plastic dissipation, whereas in composite materials, it is due to the bridging effects of fibers in the wake of the crack tip [52]. Further details on this aspect can be found in [39, Sec. 4.8] and [53, Sec. 4.3]. Another reason to consider a non-constant fracture toughness is due to nonlinear deformation because the fracture process zone may depend on the specimen geometry and the distance from boundaries [54,55]. For instance, it is well known that G_c is highly sensitive to the thickness of the test specimen [41,42]. It is worth noting that, if the sample is not sufficiently thick or the crack size is not sufficiently large, the definition of a crack length and geometry dependent fracture toughness may be arguable.

To summarize, the fracture toughness is often not a material constant. For the purposes of this work and to keep the analysis as simple as possible, we will assume G_c constant with respect to the aforementioned phenomena, but a function of a state-dependent fatigue history variable. Before introducing the fatigue model, we shortly recall in the next section the experimental evidence and key features of fatigue fracture together with Paris' law.

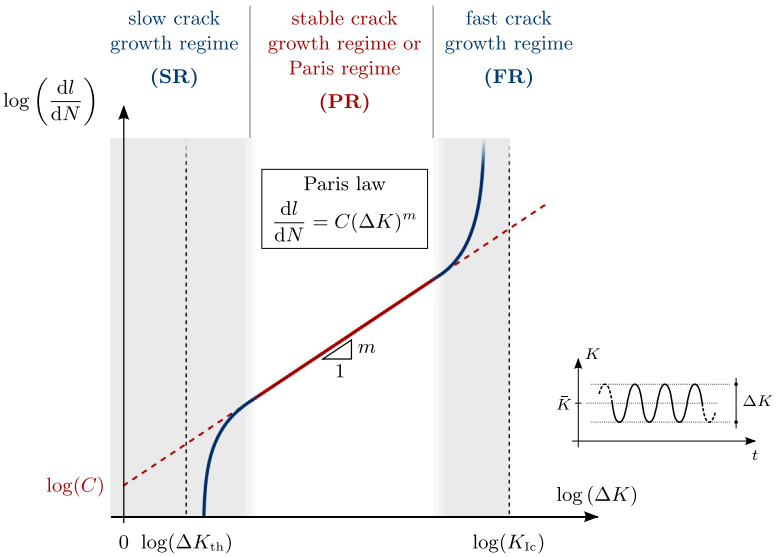

Fig. 3. Typical fatigue crack growth rate curve for a mode-I crack, cyclic loading, and constant mean value of the stress intensity factor, highlighting the three different propagation regimes and Paris' law.

2.2. Fatigue crack propagation and Paris' law

The material processes involved in the propagation of fatigue cracks are numerous, complex, and covering many length scales [1,2]. Nevertheless, at the macroscale, experiments highlight common features among many different materials. For cyclic loadings, a typical fatigue crack resistance curve is represented in a $\log - \log$ plot whose horizontal and vertical axes respectively refer to the stress intensity factor range $\Delta K := K_+ - K_-$, with K_+ and K_- being respectively the maximum and minimum stress intensity factors experienced by the material in one cycle, and the crack propagation rate with respect to the load cycles, namely, $\frac{dl}{dN}$ (Fig. 3). It is worth remarking that a single curve usually refers to a given mean stress intensity factor value $\bar{K} := (K_+ + K_-)/2$. In such response curves, three different regimes can be usually distinguished, namely: (i) a slow crack growth regime or threshold regime (SR), (ii) a stable fatigue crack propagation regime or Paris' regime (PR), and (iii) the fast crack growth regime (FR).

The SR is usually characterized by an average crack growth increment per cycle smaller than a lattice spacing and the existence of a lower threshold limit ΔK_{th}, below which cracks either remain dormant or grow at undetectable rates. In the SR, the fatigue crack growth curve is highly non-linear with a steep increase of the crack propagation rate with respect to the stress intensity factor range. The PR instead covers a wide spectrum of stress intensity factor ranges and is characterized by a linear trend. A linear relationship to describe the stable propagation of a fatigue crack was first proposed by Paris and Erdogan [56] and is widely known as Paris' law. The existence of a functional form, that is, the fact that the fatigue crack growth may depend on the stress intensity factor, was already observed in [57]. For a mode-I fatigue crack problem, Paris' law reads as follows:

$$\frac{dl}{dN} = C(\Delta K)^m, \tag{12}$$

with C and m being respectively the Paris' (law) coefficient and the Paris' (law) exponent, two material parameters characterizing the linear behavior. The FR is observed when the maximum value of the stress intensity factor experienced by the material at the crack tip approaches the critical stress intensity factor according to Griffith's fracture law (8). Indeed, the maximal stress intensity factor fixes an upper bound for the admissible stress intensity factor range during a load cycle.

Since the pioneering works of Paris, many improvements have been proposed to Paris' law in order to overcome its limitations, such as the inability to describe the initiation and the final abrupt propagation regimes or mean load effects. For instance, Forman et al. [58] modified (12) to include the asymptotic stress intensity factor limit and the mean load effect as follows:

$$\frac{dl}{dN} = \frac{C(\Delta K)^m}{(1-R)K_{Ic} - \Delta K}, \tag{13}$$

with $R := K_-/K_+$ a load parameter, usually called *fatigue stress ratio* or *fatigue load ratio*. Since the mean value of the stress intensity factor variation reads

$$\bar{K} = \frac{(1+R)}{(1-R)}\frac{\Delta K}{2}, \tag{14}$$

Forman's modification of Paris' law can be also written in terms of $\bar{K}$ as

$$\frac{dl}{dN} = C\left(\frac{\bar{K} + \Delta K/2}{K_{Ic} - K_+}\right)\Delta K^{m-1}. \tag{15}$$

It is worth noting that for Forman's modification, the slope observed in the fatigue crack propagation plot (Fig. 3) is $m-1$ for a fixed $\bar{K}$ and m for a fixed R. To also model the lower threshold, Priddle [59] proposed the following law:

$$\frac{\mathrm{d}\,l}{\mathrm{d}N} = C\left(\frac{\Delta K - \Delta K_{\mathrm{th}}}{K_{\mathrm{Ic}} - K_{+}}\right)^{m}. \tag{16}$$

The value of ΔK_{th} in this equation is supposed to be a function of R, for which different functions have been proposed in the literature, *e.g.*, by Klesnil and Lukáš [60]: $\Delta K_{\mathrm{th}} = A\,(1-R)^{\gamma}$, with A and γ two additional material parameters. An up-to-date improvement of (12) is represented by the widespread *NASGRO* equation [61,62], which reproduces many characteristic aspects of fatigue behavior, such as the nucleation, propagation, and failure phases; the crack closure effect [63]; the presence of different cracking modes; and the effect of the maximum load reached within the cycle [64], but at the cost of introducing up to 11 parameters [65]. Along these lines, many similar relations exist in the literature, for instance, considering mixed-mode loading conditions [66,67].

From the above relations, one may notice an increasing complexity of the crack growth relation over the years but still little progress with respect to an effective, predictive, and feasible application. Moreover, a rational and direct link of these phenomenological relations with Griffith's fracture evolution laws seems missing. The model presented in the following section aims at proposing a possible way to establish such a link.

2.3. The construction of the fatigue model

This section is devoted to the rational construction of the proposed phenomenological fatigue model, which takes advantage, as the models highlighted in Section 2.1.2, of considering the fracture toughness as a material function. Specifically, inspired by works [12,15] concerning the fatigue modeling of brittle fracture with the phase-field approach, we model fatigue effects by letting the fracture toughness decrease as a suitable *fatigue history variable* increases. In this regard, the modeling ingredients that we consider are the following two:

- a *fatigue history variable* ϕ;
- a *fatigue degradation function* d.

The fatigue history variable is a point-wise increasing quantity with respect to the repeated loading of the material and aims at accounting for the material *mileage*. Instead, the fatigue degradation function is continuous decreasing with respect to the fatigue history variable and is responsible of the fracture toughness degradation (mimicking the fatigue material degradation). Reasonable minimal requirements for ϕ and d are, respectively,

$$\dot{\phi} \geq 0 \tag{17}$$

and

$$d(\phi) \geq 0, \qquad \frac{\mathrm{d}}{\mathrm{d}\phi}\left(d(\phi)\right) \leq 0, \qquad \text{and} \qquad d(\phi_0) = 1, \tag{18}$$

with ϕ_0 corresponding to the value of the fatigue variable attained at the crack tip when $G = G_{\mathrm{c}}$, with external loads applied monotonically. Of course, non conventional materials, like self-healing materials [68], may demand even looser requirements. The last requirement in (18) ensures that, in case of a monotonic load, the resulting fatigue model is able to recover Griffith's fracture theory.

The *fatigue fracture toughness*[1] we then consider is given by

$$G_{\mathrm{f}}(\phi) := d(\phi)\, G_{\mathrm{c}}, \tag{19}$$

with G_{c} being the canonical fracture toughness of a virgin material. In the GSM framework, this formulation corresponds to taking a state dependent dissipation potential [69] such as

$$\mathcal{D}_{\mathrm{f}}\left(\phi;\dot{l}\right) := d(\phi)\,\mathcal{D}\left(\dot{l}\right), \tag{20}$$

with $\mathcal{D}\left(\dot{l}\right)$ defined in (4). Both $\mathcal{D}_{\mathrm{f}}\left(\phi;\dot{l}\right)$ and $\mathcal{D}\left(\dot{l}\right)$ are represented in Fig. 4.

At this point, we are able to present the abstract setting for the updated Griffith's fracture theory, which will be shown to be able to describe fatigue crack behaviors, namely:

$$\begin{cases} G \leq G_{\mathrm{f}}(\phi), & \text{(a)} \\ \dot{l} \geq 0, & \text{(b)} \\ \left(G - G_{\mathrm{f}}(\phi)\right)\dot{l} = 0, & \text{(c)} \end{cases} \tag{21}$$

at any time t. With respect to GSM, problem (21) becomes

$$-\frac{\partial \mathcal{P}}{\partial l} \in \partial_{\dot{l}}\mathcal{D}\left(\phi;\dot{l}\right) \tag{22}$$

at any time t.

In the next section, specific constitutive choices for ϕ and d are proposed and discussed.

[1] In case of a non-prescribed crack path, the fatigue fracture toughness is also defined over the entire sound domain, that is, $G_{\mathrm{f}}(\boldsymbol{x},t) := d(\phi(\boldsymbol{x},t))\,G_{\mathrm{c}}$.

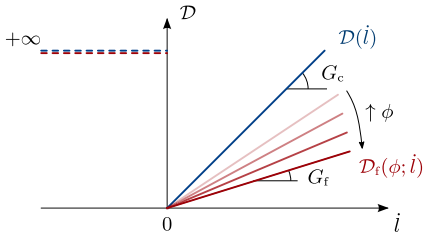

Fig. 4. Fracture (blue) and fatigue (red) dissipation potentials.

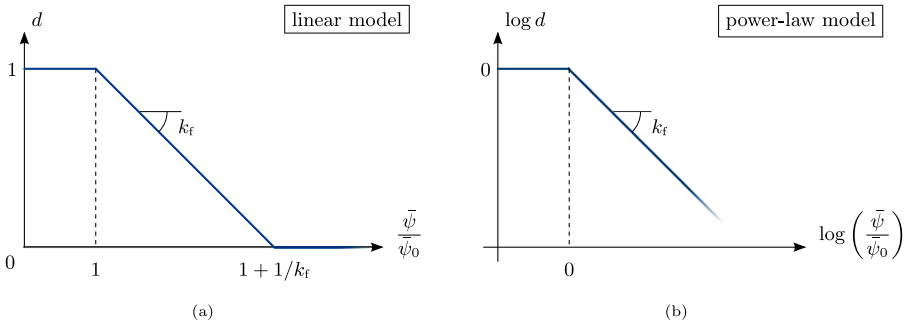

Fig. 5. Representation of the fatigue degradation function models: (a) the linear model and (b) the power-law model.

2.4. Some specific fatigue degradation functions and fatigue history variables

In this section, specific fatigue degradation functions and fatigue history variables are introduced and discussed. Most of them will be analyzed and explored in the subsequent section (Section 3), where specific examples will be considered.

2.4.1. Fatigue degradation function

Starting from the works of [12,15], several different expressions for the fatigue (degradation) function have been proposed, such as polynomial, rational, and logarithmic ones [24], all having in common the minimal requirements (18).

For the sake of simplicity, to enforce the last property in (18), we define the fatigue degradation function through an upper bound as follows:

$$d(\phi) := \begin{cases} 1, & \text{if } \phi \le \phi_0, \\ f(\phi), & \text{if } \phi > \phi_0, \end{cases} \tag{23}$$

with f being an auxiliary function, hereafter simply labeled *fatigue function*. Clearly, continuity implies $f(\phi_0) = 1$, with ϕ_0 being the limit value of the fatigue history variable at critical monotonic load.

In this work, two simple expressions for f, alternative to each other and satisfying conditions (18), are considered:

- *linear model*

$$f_l(\phi) := \max\left\{0, 1 + k_f\left(1 - \frac{\phi}{\phi_0}\right)\right\}; \tag{24}$$

- *power-law model*

$$f_p(\phi) := \left(\frac{\phi}{\phi_0}\right)^{-k_f}; \tag{25}$$

with $k_f > 0$ being the *fatigue degradation parameter*. The division of ϕ by ϕ_0, appearing in (24) and in (25), will allow us to capture the monotonic fracture limit. The corresponding fatigue degradation functions are represented in Fig. 5.

The resulting fatigue degradation function can be further modified by including a lower bound that mimics an endurance limit effect. Nevertheless, in this framework, the correct modeling of the endurance limit is still an open issue since different approaches are potentially possible for its description. For the purposes of this work and to keep the presentation as simple as possible, endurance limits are not considered.

2.4.2. Fatigue history variable

At each point and at any instant, the fatigue history variable aims at representing the amount of mechanical *stimuli* the material point has incrementally experienced during its entire life time. Since aging phenomena are here excluded, no fatigue degradation should in general be observed, and correspondingly no fatigue history variable evolution should occur, if the strain or the stress tensor (the only mechanical quantities characterizing the state of a material point in Griffith's fracture theory) does not change in time, neither with respect to its principal values nor with respect to its principal directions. In practice, as anticipated in Section 2.3 and discussed in Section 2.5, several choices are possible for the definition of the fatigue history variable and more than one can be considered. The introduction of more history variables seems natural, to not say necessary, in case of multi-axial and non-proportional loading conditions [3]. In the present work, a single scalar fatigue history variable is considered, which we assume to be based solely on the history of the internal potential energy density, namely,

$$\phi = \phi\left({}^{t}\psi\right) =: \bar{\psi}. \tag{26}$$

We do not claim (26) to be the best possible choice, but in this simplified context and for the purposes of this work, this history variable turns out to have all the required features to endow Griffith's fracture model with the ability to describe typical fatigue crack propagation behaviors.

To enter more in detail, the general functional structure we assume for the fatigue history variable reads

$$\bar{\psi}\left(t, \boldsymbol{x}, {}^{t}\hat{\Gamma}, {}^{t}\psi\right) = \int_0^t g\left(\boldsymbol{x}, \hat{\Gamma}(\tau), \psi(\tau,\boldsymbol{x}), \dot{\psi}(\tau,\boldsymbol{x})\right) \mathrm{d}\tau, \tag{27}$$

defined at any material point $\boldsymbol{x} \in \Omega \setminus \hat{\Gamma}(t)$.

In order to fulfill requirement (17), the scalar valued integrand is assumed always non-negative, $g \geq 0$, and therefore, $\bar{\psi}$ is a non-decreasing function. Moreover, g is such that $\bar{\psi}$ is rate-independent, that is, g one-homogeneous with respect to $\dot{\psi}$. Therefore, if ψ is constant, $g = 0$. The function g then represents a kind of generalized fatigue internal variable rate and $\bar{\psi}$ its accumulation.

According to the elastic solution discussed in Section 2.1.1 and to common experimental evidence, we ask the fatigue variable to comply with the following requirements:

1. Deal with the singularity of ψ at the crack tip;
2. Capture under which material loading conditions the fatigue degradation evolves, or, in other words, accumulation should occur;
3. Take into account mean stress effects;
4. Describe the PR with arbitrary m.

More involved fatigue effects, as those deriving from considering more complex loading conditions, such as multi-axial loadings, can be easily be embedded in this framework, for instance by considering additional fatigue variables based on energy splits. Nevertheless, these additional features, although very important under a practical viewpoint, are not considered here for sake of brevity and their investigation is left to future works.

In the present setting (Fig. 1) where the crack path is prescribed, the set $\hat{\Gamma}(t)$ and the position of the crack tip $\boldsymbol{x}_l$ can be directly related to the actual crack length $l(t)$ and the material points on the crack path identified by the crack arc-length s. Indeed, for describing the fatigue crack evolution, it is sufficient to evaluate the fatigue variable on the sound part of the crack $\check{\Gamma}$, where the fatigue enhanced Griffith's crack conditions (21) are enforced. Accordingly, (27) can be expressed as

$$\bar{\psi}\left(t, s, {}^{t}l, {}^{t}\psi\right) = \int_0^t g(r, \psi(\tau,r), \dot{\psi}(\tau,r))\, \mathrm{d}\tau, \tag{28}$$

with $r = s - l(\tau)$ and $\psi(\tau, r) = \psi(\tau, \boldsymbol{x}_r)$. Eq. (28) is clearly valid only on $\check{\Gamma}(t)$. In addition, it is worth noting that the expression (27) is well defined on all material points of the sound domain. Consequently, it can be considered as a starting point for problems with an unknown crack path.

Among the many, to not say endless, possible functional choices for g, we decide to consider one obtained as a composition of simple functions, each of them aiming at modeling one of the specific 1 - 4 features listed above. This composition allows us to understand *step by step* all the features of the model and the role of each material parameter. Specifically, the following functional structure is assumed:

$$g(r, \psi(\tau,r), \dot{\psi}(\tau,r)) := g_4\left(\psi^*\left({}^{t}\tilde{\psi}\right)\right) \cdot g_3\left(\tilde{\psi}\right) \cdot g_2\left(\dot{\tilde{\psi}}\right), \qquad \text{with} \qquad \tilde{\psi} := g_1(r, \psi(\tau,r)). \tag{29}$$

Hereafter, the four functions g_i of (29) are introduced and their roles highlighted. In particular, each function g_i aims at capturing the ⓘth feature listed above.

Function g_1. The function g_1 aims at dealing with the energy singularity at the crack tip. It formally introduces the FDZ highlighted in Fig. 1, which is characterized by the fatigue length ℓ_{f}. Accordingly, we assume

$$g_1(r, \psi) = h(\|\boldsymbol{r}\|) \sqrt{\|\boldsymbol{r}\|}\, \sqrt{\psi}, \tag{30}$$

with $\boldsymbol{r} := \boldsymbol{x}_r - \boldsymbol{x}_l$. Under the mathematical point of view, the term $\sqrt{\|\boldsymbol{r}\|}$ smooths the energy singularity at the crack tip to a finite value, whereas the function $h(\|\boldsymbol{r}\|)$ describes the decay of the smoothed energy with respect to the fatigue material internal length. Specifically, in view of (6),

$$\lim_{r\to 0} \|\boldsymbol{r}(r)\|\, \psi(t, \boldsymbol{r}(r)) = k_\psi \quad (< +\infty). \tag{31}$$

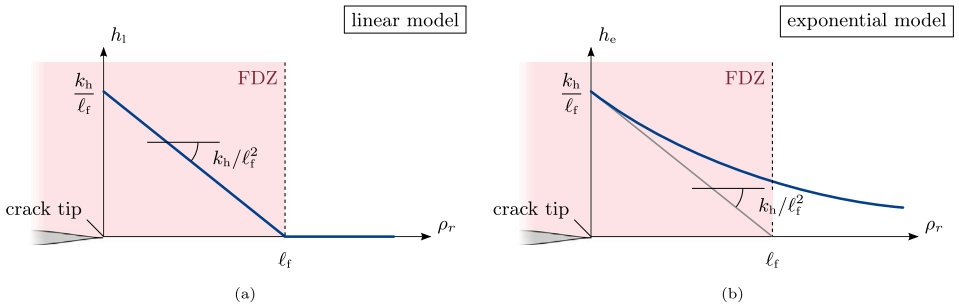

Fig. 6. (a) linear and (b) exponential model for the fatigue threshold function.

Since $k_\psi \propto K_{\mathrm{I}}^2$, the square root in (30) will let appear the stress intensity factor with power one and not its square. Instead, the function $h(\rho_r)$, where $\rho_r := \|\boldsymbol{r}\|$, is called *fatigue threshold function* and embeds the information of the fatigue degradation zone through the fatigue length ℓ_{f}, tuning the decay shape of $\sqrt{\|\boldsymbol{r}\|}\sqrt{\psi}$ from the crack tip. It is reasonable to assume $h(\rho_r)$ continuous and owning the following properties:

$$\lim_{r\to 0} h(\rho_r) = \frac{k_{\mathrm{h}}}{\ell_{\mathrm{f}}} \quad (<\infty), \qquad h'(\rho_r) \le 0, \qquad \lim_{\|\boldsymbol{r}\|\to+\infty} h(\rho_r)\sqrt{\|\boldsymbol{r}\|} < +\infty, \tag{32}$$

with k_{h} being a material parameter. It is worth remarking that the manipulation performed on the elastic energy density is similar to the averaging operation done in the strain energy density criterion (S-criterion) [70].

With these properties in mind, the resulting $\tilde{\psi}$ field will be referred to as the *smoothed internal energy density* or simply *smoothed energy*. Clearly, in case of a straight crack, $\|\boldsymbol{r}\| = \rho_r = r$. Instead, for a non-straight but smooth crack path, as it has been assumed, $\lim_{r\to 0} \|\boldsymbol{r}(r)\|/r = 1$. Hence, for a sufficiently small r, $\|\boldsymbol{r}(r)\| \sim r$.

In this work, two simple expressions for $h(\rho_r)$, alternative to each other and satisfying conditions (32), are considered:

- *linear model*

$$h_{\mathrm{l}}(\rho_r) = \begin{cases} \dfrac{k_{\mathrm{h}}}{\ell_{\mathrm{f}}}\left(1 - \dfrac{\rho_r}{\ell_{\mathrm{f}}}\right), & \text{if } 0 \le \rho_r \le \ell_{\mathrm{f}}, \\ 0, & \text{if } \rho_r > \ell_{\mathrm{f}}; \end{cases} \tag{33}$$

- *exponential model*

$$h_{\mathrm{e}}(\rho_r) = \begin{cases} \dfrac{k_{\mathrm{h}}}{\ell_{\mathrm{f}}}, & \text{if } \rho_r = 0, \\ \dfrac{k_{\mathrm{h}}}{\ell_{\mathrm{f}}}\dfrac{\left(1 - e^{-2\rho_r/\ell_{\mathrm{f}}}\right)}{2\rho_r/\ell_{\mathrm{f}}}, & \text{if } \rho_r > 0; \end{cases} \tag{34}$$

both of them continuous over $[0, +\infty)$. The material constant k_{h} is directly proportional to the value of the smoothed energy at the crack tip. A qualitative representation of the functions (33) and (34) is provided in Fig. 6.

As motivated in the introduction of this section, the physical reason for the introduction of the fatigue degradation zone, identified by the fatigue length ℓ_{f}, relies on the fact that, regardless the actual material, a linear elastic behavior close to the crack tip is always unrealistic. Nevertheless, for sake of easiness, we try to still rely on a linear-elastic framework and use the accumulation of an internal potential energy density based variable as an indicator of fatigue degradation.

Let us briefly discuss now the main difference between the linear and exponential models adopted for h:

- the linear model weights the internal potential energy density with the smoothed singularity up to a finite distance from the crack tip. Therefore, for a distance greater than ℓ_{f}, no material degradation due to fatigue will occur.
- the exponential model weights the internal potential energy density up to an infinite distance from the crack tip. Therefore, the material degrades in any point where a non vanishing energy variation will occur.

It is worth noticing that a model based on a fatigue threshold function like the exponential one, that is, a function that allows the fatigue variable to evolve also in sound parts of the domain far away from the crack tip, could be the key for capturing fatigue crack initiation, as described by the Wöhler curves [15].

Function g_2. The function g_2 aims at discriminating for which material loading conditions the fatigue variable should increase, that is, the loading conditions for which fatigue material degradation occurs.

Since our subsequent analyses will be focused on *simple loadings*, that is, loadings for which the loading direction is kept fixed during the entire evolution, we will only consider

$$g_2 = (\square)^+ . \tag{35}$$

In case of non-proportional loading conditions, a more involved definition should be prescribed, since, for instance, the effect of the reorientation of the principal strain/stress directions may become significant [3]. Another possible effect that can be modeled by g_2 is the distinction between compressive and tensile states on the fatigue variable evolution. This will of course require explicitly considering the stress state in the definition of the fatigue variable. To keep the presentation of the model as simple as possible, we do not discuss this occurrence in the present work and restrict our examples to loadings inducing only tensile states.

Function g_3. The function g_3 aims at considering the effects of the mean load on the fatigue accumulation. We consider for g_3 the following power law:

$$g_3(\tilde{\psi}) = \tilde{\psi}^p, \tag{36}$$

with $p > 0$. For $p = 0$, no mean load effects will be observed.

Function g_4. The function g_4 aims at weighting the fatigue variable accumulation with respect to the amount of consecutive fatigue loading. Several definitions of increasing complexity may be considered.

A first simple possibility to quantify the amount of consecutive fatigue loading is to introduce an auxiliary history variable ψ^*. This can be effectively done once the following time dependent set has been introduced:

$$\check{\mathcal{T}}(t) := \left\{ \check{t} \le t \text{ for which } \exists t^- < \check{t} \ : \forall \tau \in \left[t^-, \check{t}\right], \ \dot{\tilde{\psi}}(\tau) \le 0 \text{ and } \exists \tau^* \in \left[t^-, \check{t}\right] \ : \dot{\tilde{\psi}}(\tau^*) < 0 \right\}, \tag{37}$$

representing the time intervals which correspond to unloadings. Then,

$$\psi^* \left({}^t\tilde{\psi}, t \right) := \int_{\check{t}}^{t} \dot{\tilde{\psi}}(\tau) \mathrm{d}\tau, \quad \text{with} \quad \check{t} = \max \left\{ \{0\} \cup \check{\mathcal{T}}(t) \right\}. \tag{38}$$

The quantity $\check{t}$ corresponds to the last time instant for which an unloading stage has occurred. Consequently, a feature of (38) is that as soon as unloading occurs, ψ^* instantaneously vanishes. It is worth noting that this kind of *reset* of the variable occurs only during unloading and not if, during a loading stage, the load is kept constant for a while. Indeed, during a loading stage, if the load is kept constant, ψ^* also remains constant and continues to increase as soon as the load is increased again.

Clearly, many other definitions are possible, such as a progressive decrease to zero when the material is unloaded. The behavior just described can be obtained by considering

$$\psi_c^* \left({}^t\tilde{\psi}; t \right) := \left(\psi_c^\star \left({}^t\tilde{\psi}; [\check{t}, t] \right) \right)^+, \tag{39}$$

with

$$\check{t} = \max \left\{ \{0\} \cup \check{\mathcal{T}}_c(t) \right\}, \qquad \psi_c^\star \left({}^t\tilde{\psi}; [t_i, t_j] \right) = \int_{t_i}^{t_j} c \left(\operatorname{sign}(\dot{\tilde{\psi}}(\tau)) \right) \ \dot{\tilde{\psi}}(\tau) \mathrm{d}\tau, \tag{40}$$

and

$$\check{\mathcal{T}}_c(t) := \left\{ \check{t} \ \text{ for which } \ \check{t} \in \check{\mathcal{T}}(t) \ \text{ and } \ \forall t^* (\in \check{\mathcal{T}}(t)) < \check{t}, \ \psi_c^\star \left(t^*, \check{t} \right) < 0 \right\}. \tag{41}$$

In (39), the function $c(x)$ is given by

$$c(x) := \begin{cases} c^+, & \text{if } x = 1, \\ c^-, & \text{if } x = -1, \end{cases} \tag{42}$$

with $-c^- > c^+ > 0$.

A visual intuition of the behaviors of ψ^* and ψ_c^*, together with the sets $\check{\mathcal{T}}(t)$ and $\check{\mathcal{T}}_c(t)$, are provided in Fig. 7(a) and Fig. 7(b), respectively. The history variable ψ_c^* allows the fatigue history variable to partially increase during unloadings, resulting in a faster fatigue degradation. Also, in case of cyclic loadings with partial unloadings within one cycle, as after t_{i+1} in Fig. 7, ψ_c^* will favor a faster fatigue degradation with respect to ψ^*. Such a difference may have a significant impact when complex cyclic, multi-axial or non-proportional loadings are considered. It is also worth remarking that crack closure effects could easily be included through a slight modification of these new auxiliary history variables.

Once the history variable (38) or (39) has been introduced, we define the *consecutive fatigue loading function* g_4 as a power law, similar to (36):

$$g_4(\psi^*) := (\psi^*)^q. \tag{43}$$

As we will show in Section 3, the exponent q is directly linked to the Paris' law exponent.

No constants are considered in front of g_3 and g_4 because they can be normalized and condensed into k_h in (33)–(34). It is also worth noting that for some common choices of g_2 and g_4, the effect of g_2 on the fatigue history variable may be already expressed by g_4. Nevertheless, we decide to always keep well distinct the contribution of the two functions since they conceptually refer to two different features of the model.

Now that all functions have been explicitly introduced, it is easy to note that the definition of the fatigue variable is rate-independent. Thus, the introduced fatigue model in insensitive to time-scaling.

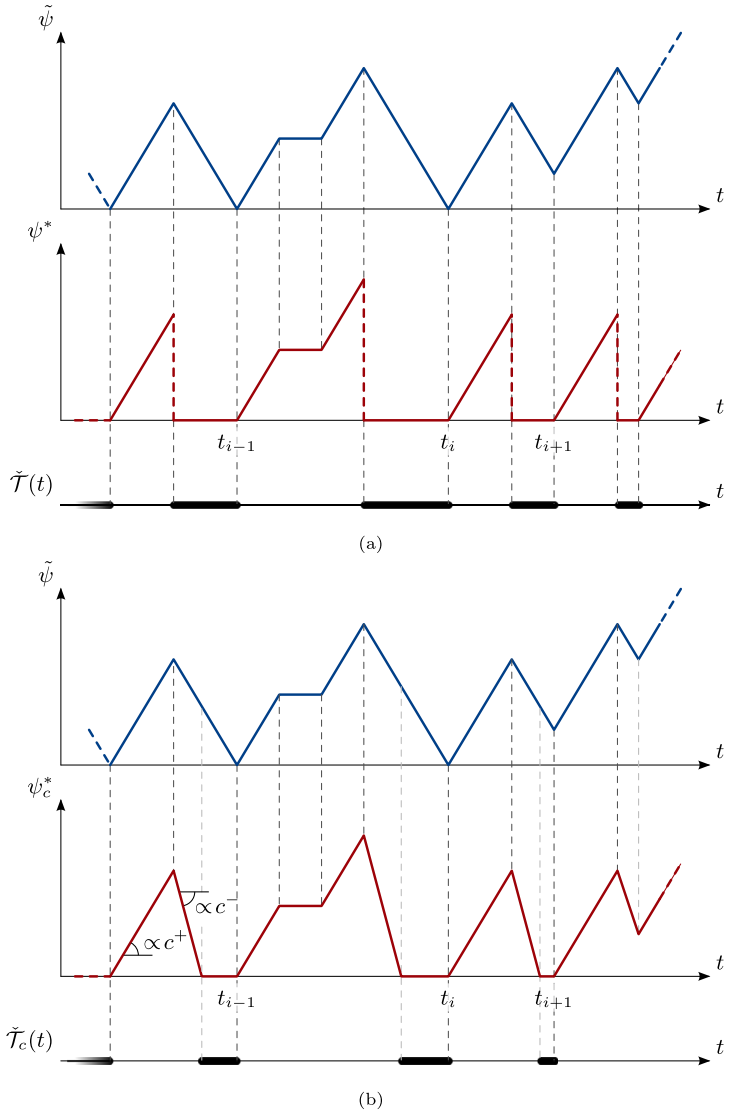

Fig. 7. Additional history variable for weighting consecutive loading: (a) without unloading contribution and (b) with unloading contribution.

2.5. Towards a variational fatigue phase-field fracture model

As discussed in Section 1, this work aims at providing a sound theoretical ground on top of which a new generation of phase-field models able to describe fatigue fracture can be built. To this aim and without the presumption of providing an exhaustive survey, we wish to highlight in this section existing phenomenological phase-field models that have adopted the concept of toughness degradation for the description of fatigue crack propagation. Those that explicitly define a fatigue history variable and/or a fatigue degradation function, and therefore conceptually fit the modeling framework presented in Section 2, are presented in Table 1. Specifically, for each model, we report the following information: the work reference, the fatigue variable, the expressions for the fatigue history variable and the fatigue degradation function, the main features, and the underlying material behavior besides fatigue and fracture.

The concept of toughness degradation to model fatigue has also been adopted in [71]. In contrast with the models mentioned in Table 1, in that work, the evolution law for the toughness degradation is directly prescribed through either the *variable critical energy model*, acting on the homogeneous part of the phase-field dissipative term, or through the *γ-model* acting on the entire phase-field dissipative term. Other approaches to model fatigue effects within a gradient-damage framework, worth being mentioned, are proposed by [10], where, similar to [31], an additional energetic term increasing the phase-field driving force is introduced;

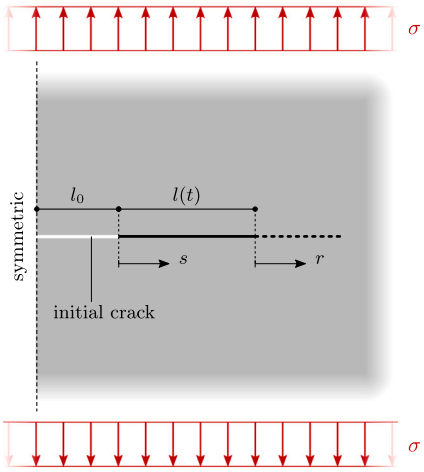

Fig. 8. Geometry and boundary conditions of the IPSC under mode-I loading.

by [72], where the evolution law for the damage variable accounting for fatigue effects is directly prescribed; or by [36], where the volumetric elastic energy is chosen as a fatigue variable and an evolution law for the toughness degradation is directly prescribed through an ordinary differential equation in terms of the load cycle number.

From this brief overview, it is clear that the development of fatigue phase-field models is at dawn and that many key issues still need to be explored, such as, for instance, the effect of multi-axial loadings and computational efficiency. However, we focus here on a more fundamental limitation: the absence of a link between fatigue-enhanced phase-field models and a Griffith-type fracture theory. The lack of such a link renders these phase-field models not fully consistent with the original spirit of the variational approach to fracture [8], since they do not descend from a rigorous variational regularization process. We thus envisage a new generation of fatigue phase-field models that are rigorously derived from a suitable energy functional, with the dissipative behavior relying on a fatigue fracture toughness and fatigue history variable of the type (19) and (26), respectively.

3. Illustrative examples

3.1. The mechanical problem

The mechanical problem we consider for highlighting key features and validating the outcomes of the fatigue model proposed in Section 2 is the *infinite plate with a symmetric crack* (IPSC) subjected to mode-I loading. The reasons to consider such an example are twofold. On one hand, this is one of the few problems for which the exact analytical solution is available. This will allow us, for instance, to compare the fatigue effects of the exact solution with the fatigue effects emerging from the use of only the near-tip K-stress solution. On the other hand, the expression of the stress intensity factor K_{I} with respect to the geometric quantities involved in the problem and the boundary conditions is particularly simple, allowing for compact analytical results.

It is worth it to immediately remark that, as will be clear from the forthcoming analyses, the adaption of the model to other problems with a single fracture is straightforward. In this regard, a plethora of solutions of canonical fracture problems can be found in [67].

3.1.1. Geometry, boundary conditions, energy release rate, and stress intensity factor

The geometry of the IPSC together with the associated mode-I loading boundary conditions are presented in Fig. 8, with the far field stress σ being a time dependent quantity.

The crack-length dependent energy release rate at a given stress intensity factor is given, for mode-I loading, by (7), namely

$$G = k_{\mathrm{G}} K_{\mathrm{I}}^2 = k_{\mathrm{G}}\, \pi\, l\, \sigma^2, \tag{44}$$

with $k_{\mathrm{G}} = 1/E$ for plane-stress and $k_{\mathrm{G}} = (1-\nu^2)/E$ for plane-strain. Eq. (44) is usually referred to as Irwin's formula [76]. Accordingly, the monotonic critical stress intensity factor is linked with the fracture toughness by

$$K_{\mathrm{Ic}} = \sqrt{\frac{G_{\mathrm{c}}}{k_{\mathrm{G}}}}. \tag{45}$$

The exact stress solution and its associated near-tip approximation, together with their associated elastic energy density fields, are reported in the Appendix.

Table 1
Phase-field models based on the fracture toughness degradation concept for the description of fatigue cracks. κ_i and p are material constants; H is the *Heaviside* function; α is the phase-field variable; ψ is the degraded phase-field free energy; ψ_0 is the non-degraded phase-field free energy; ψ^+ is the positive part of the elastic energy density according to the adopted energy split; ψ_{el} and ψ_{pl} are, respectively, the elastic and plastic free energy contributions; $\mathcal{H}(\psi^+)$ is Miehe's history variable [73]; $I_1 = \text{tr}\,(\boldsymbol{C})$ is the first invariant of the Cauchy–Green strain tensor. (↑) innovative feature, (∘) peculiar feature, (↓) possible limit of the model.

References	Fatigue variable ξ	Fatigue history variable $\phi(\xi)$	Fatigue degradation function $d(\phi)$ or $f(\phi)$	Main key features and limits of the model	Material behavior[a]
[15] - Carrara et al. (2020)	ψ^+	$\frac{1}{\kappa_1^p}\int_0^t H(\dot{\xi})\,\xi^p\,\dot{\xi}\,\mathrm{d}\tau$ with $p = 0/1$	$\begin{cases} 1, & \text{if } \phi \le \kappa_2 \\ \left(2\kappa_3/(\phi+\kappa_3)\right)^2, & \text{if } \phi > \kappa_2 \end{cases}$, or $\begin{cases} 1, & \text{if } \phi \le \kappa_2 \\ \left(1-\kappa_4 \log\left(\phi/\kappa_2\right)\right)^2, & \text{if } \kappa_2 < \phi \le \kappa_2 10^{\frac{1}{\kappa_3}} \\ 0, & \text{if } \phi > \kappa_2 10^{\frac{1}{\kappa_3}} \end{cases}$	↑first phase-field model to recover Paris' fatigue crack regime ↑unifying approach to describe Wöhler curves and Paris' fatigue crack regime ∘ mean load effects only qualitatively captured ↓inability to tune Paris' law exponent ↓internal length dependent fatigue crack rate	Elastic
[74] - Hasan and Baxevanis (2021)	$\mathcal{H}(\psi^+)$	$\int_0^t H(\psi^+ - \kappa)\left(\langle\dot{\psi}^+\rangle - \dot{\xi}\right)\mathrm{d}\tau$	$\frac{1}{1+\kappa\phi^p}$	↑fatigue effects on crack topology investigation ↑endurance limit introduction ∘ low-cycle fatigue ↓no fatigue effects during history variable evolution ↓mesh size dependent fatigue history variable ↓internal length dependent fatigue crack rate	
[24] - Yin et al. (2021)	ψ_0^+	$\int_0^t g(\alpha)H(\dot{\xi})\lvert\dot{\xi}\rvert\,\mathrm{d}\tau$	$\begin{cases} 1, & \text{if } \phi \le \phi_{\text{cr}} \\ \left(1-\kappa_4 \log\left(\frac{\phi}{\kappa_2}\right)\right)^2, & \text{if } \kappa_2 < \phi \le \kappa_2 10^{\frac{1}{\kappa_3}} \\ 0, & \text{if } \phi > \kappa_2 10^{\frac{1}{\kappa_3}} \end{cases}$	↑finite strains setting ↑mesh size and internal length independent fatigue crack rate ↑material force regularization ↓no Paris' law parameters investigation	
[21] - Seiler et al. (2020)	D (a cycle wise phenomenologically computed variable)		$(1-\kappa)(1-\phi)^p + \kappa$	↑elasto-plastic stress-revaluation without an explicit elasto-plastic material model ↓no Paris' law parameters investigation ↓complex computational flow ↓internal length dependent fatigue crack rate	Elasto-Plastic
[17] - Ulloa et al. (2021)	$\psi_{\text{el}}^+ + \psi_{\text{pl}}$	$\int_0^t H(\dot{\xi})\dot{\xi}\,\mathrm{d}\tau$	same as f_2 of Carrara et al. [15]	↑first elasto-plastic material model to investigate fatigue effects ↑HCF and LCF fatigue regimes ↓no quantitative experimental comparisons ↓internal length dependent fatigue crack rate ↓no Paris' law parameters investigation	
[18] - Seleš et al. (2021)	$\psi_{\text{el}0}$	$-\int_0^t H(-\dot{\xi})\dot{\xi}\,\mathrm{d}\tau$	$\begin{cases} \left(1-\phi/(\phi+\kappa_1)\right)^2, & \text{for}\phi \in [0,+\infty], \text{or} \\ \left(1-\phi/(\kappa_1)\right)^2, & \text{for}\phi \in [0,\kappa_1], \text{or} \\ \left(\kappa_2 \log(\kappa_1/\phi)\right)^2, & \text{for}\phi \in [\kappa_1, 10^{\frac{1}{\kappa_2}}\kappa_1] \end{cases}$	↑HCF and LCF fatigue regimes ∘ fatigue degradation during unloading ↓no Paris' law parameters investigation ↓internal length dependent fatigue crack rate	

(*continued on next page*)

Table 1 (*continued*).

References	Fatigue variable ξ	Fatigue history variable $\phi(\xi)$	Fatigue degradation function $d(\phi)$ or $f(\phi)$	Main key features and limits of the model	Material behavior[a]
[31] - Loew et al. (2020)	ψ	$\int_0^t H(\dot{I}_1)H(1+\kappa_1 f_\kappa)\dot{\xi}\,\mathrm{d}\tau$ with $f_\kappa = \max(p-\kappa_2, 0)$	Fatigue effect modeled as an additional phase-field driving force	↑first elasto-viscosity model to include fatigue effects ↑finite strains setting ↑computational acceleration schemes ↓many material parameters and functions to set up	Elasto-Viscous
[75] - Simoes and Martínez-Pañeda (2021)	ψ	Same as [15] with $p = 0$ and $f = f_1$		↑first model to couple superelastic SMA behavior with fatigue effects ↑monolithic numerical scheme to speed up computations ↓no fatigue modeling improvements compared to previous works	SMA

[a]Besides fatigue and fracture.

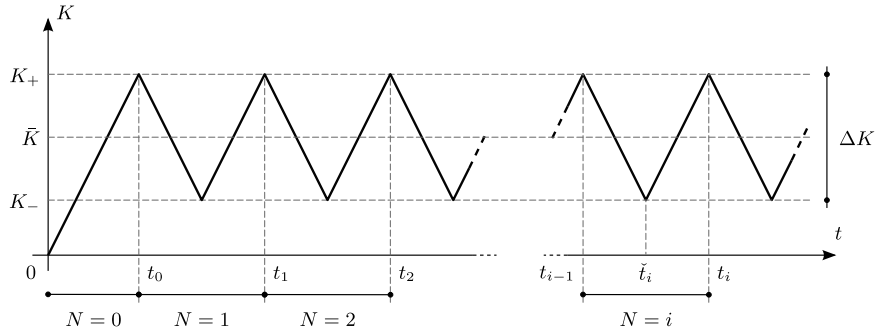

Fig. 9. A simple tension–tension K-cyclic loading.

3.1.2. Loading conditions

For the present example, only *simple loadings*, that is, loadings for which the loading direction is kept fixed during the entire evolution, are considered. In addition, we restrict simple loadings to those that will never induce compressive contact stresses along the crack path and that are cyclic with constant amplitude.

Accordingly, the following quantities are usually considered to characterize a cyclic loading:

$$\Delta K = K_+ - K_-, \quad \bar{K} = \frac{K_+ + K_-}{2}, \tag{46}$$

in terms of stress intensity factors, or

$$\Delta\sigma = \sigma_+ - \sigma_-, \quad \bar{\sigma} = \frac{\sigma_+ + \sigma_-}{2}, \tag{47}$$

in terms of the far field stresses, together with fatigue load ratio

$$R = \frac{\sigma_-}{\sigma_+} = \frac{K_-}{K_+}. \tag{48}$$

where $\square_+$ and $\square_-$ are the maximum and minimum values attained by $\square$ during a cycle.

Specifically, the class of loadings that we take into account are referred to as *simple tension–tension cyclic loadings*. For such a class, two different loading conditions are considered:

- *K-cyclic loading*, for which the external load is continuously adapted in order to keep the stress intensity factor variation constant, namely, $\Delta K = \text{constant}$;
- *σ-cyclic loading*, where the far field stress variation is kept constant, namely, $\Delta\sigma = \text{constant}$.

The *simple tension–tension cyclic loading* conditions are fulfilled with

$$0 \le K_- < K_+ \quad \text{and} \quad 0 \le \sigma_- < \sigma_+ \tag{49}$$

or, equivalently, by assuming

$$0 \le R < 1. \tag{50}$$

Due to the rate-independent model behavior, only the sequence and intensity of peaks and valleys will determine the material response, while the applied loading rate does not play a role. This fact allows us to consider linear interpolations between these limit points. A typical loading diagram of a *simple tension–tension K-cyclic loading* is depicted in Fig. 9, where limit points and time interval labels are also represented. The diagram for a *simple tension–tension σ-cyclic loading* is exactly the same, provided that the stress intensity factor label K is replaced by the stress label σ. Of course, regardless of the kind of load, an initial vanishing load level is always assumed.

3.2. The fatigue crack propagation stages

The analysis conducted in this section aims at describing in detail the fatigue crack evolution of a virgin material subjected to a simple tension–tension σ-cyclic load for a very simple model. Specifically, we consider here the linear threshold function (33), no mean load and consecutive accumulation effects, that is, $p = q = 0$, the linear fatigue function (24), and $\ell_{\mathrm{f}} \ll \ell_{\mathrm{k}}$, this condition allowing us to consider only the K-stress solution. The response of such a simple model will already exhibit features common to more involved models later considered. For instance, it turns out that the fatigue crack evolution consists of three peculiar stages, namely:

- the *initial accumulation stage*;

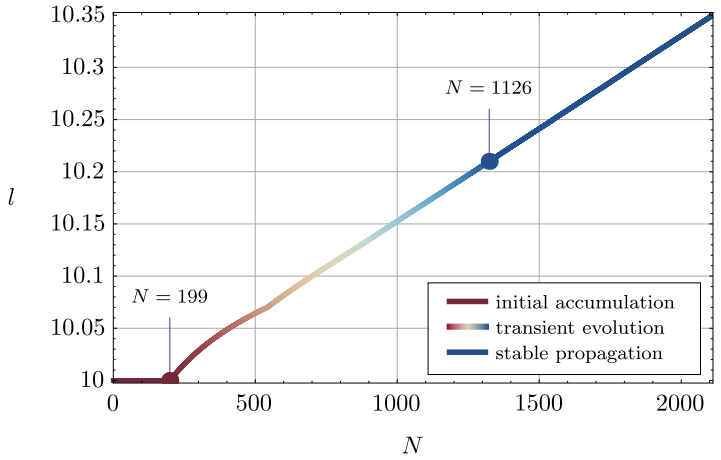

Fig. 10. Crack length evolution with respect to the number of cycles.

- the *transient evolution stage*;
- the *stable propagation stage*.

For the example presented in this section, the following parameters have been chosen: initial crack length $l_0 = 10$; fatigue length $\ell_f = 0.007 l_0$ ($\approx 1/10\,\ell_k$), with ℓ_k computed according to (9) and (11) with $\bar{\Lambda} = 95\%$; fracture toughness $G_c = 10$; and all other constants of unitary value, except for Poisson's ratio ($\nu = 0.25$). Concerning the cyclic load, the far field stress is such that $\sigma_- = 0$ and $\sigma_+ = 0.01\sigma_0$, with $\sigma_0 := K_{Ic}/\sqrt{\pi l_0}$ being the limit far field stress for a monotonic load. Consequently, we have $\Delta\sigma = 0.01\sigma_0$ and $R = 0$.

Let us briefly describe the simple numerical solution strategy adopted to derive the evolution. At any load peak, that is, at any t_i, condition (21a) at $r = 0$ is checked. If $G \leq G_f(\phi)$, no crack propagation occurs, and the fatigue history variable is updated. If, instead, $G > G_f(\phi)$, the current solution is not admissible and a crack evolution must have occurred. The crack length advancement is then sought by enforcing $G = G_f(\phi)$ at the unknown crack tip location as a function of l and the fatigue history variable updated accordingly.

Fig. 10 and Fig. 11 report, respectively, the crack length and the crack rate evolutions with respect to the number of cycles, whereas Fig. 12 highlights the evolution of the fatigue variable profile with respect to the crack length. Up to $N = 199$, the crack does not evolve since the evolution condition (21a) is not met as an equality. Nevertheless, during this stage, the fatigue variable constantly increases at each cycle with a linear behavior, as evident from the red lines in Fig. 12. Accordingly, we call this stage *initial accumulation stage*. At $N = 199$, the fatigue fracture toughness has sufficiently diminished due to the fatigue variable accumulation, such that, during this cycle, condition (21a) is met as an equality and the crack starts to propagate. This change in the response is highlighted with a dark red point marker in the plots. After this limit, the crack starts to propagate at a slightly oscillating rate, as clear from Fig. 11, until it stabilizes at approximately the state highlighted with a dark blue point marker ($l \approx 3\ell_f$ and $N \approx 1493$). During this period, the fatigue history variable profile progressively changes shape from linear to quadratic as the crack length increases. A gradient color ranging from dark red to dark blue is used to emphasize this transition. Accordingly, this stage is here called *transient evolution stage*. After this second limit point, a steady response is achieved, referred to as *stable propagation stage*, where the fatigue crack propagation rate and the fatigue variable profiles stay approximately constant. Note that the crack propagation rate slightly increases during the stable propagation stage due to the fact that both the stress intensity factor limits $K_\pm$ and mean value $\bar{K}$ increase as the crack evolves, even though the stress load limits are kept constant.

Nevertheless, plotting the fatigue crack propagation rate against the stress intensity factor variation, as done in Fig. 13, unveils convergence towards a stabilized response. This behavior is a prelude for the results of the next section, that is, the closed form relation between crack propagation rate and the stress intensity variation during stationary evolution (76), hereby represented with a gray curve in the same plot.

It is worth noting that during the *transient evolution stage*, the crack propagates initially faster (dark red gradient part of the curve) than during the *stable propagation stage* because the fatigue variable profile at the first limit point (dark red linear profile) is greater than the profile at the second limit point (dark blue quadratic profile), that is, at incipient stable propagation. This means that the material ahead of the crack tip degrades more before triggering fatigue crack propagation than during the steady propagation stage.

With this example, the main evolution features of the present fatigue model have been highlighted. In the forthcoming sections, more details on the role of each material parameter will be provided.

3.3. The stationary fatigue crack propagation regime and link to Paris' law

In this section, a stationary fatigue crack propagation regime is considered. Differently from the stable propagation stage illustrated in the previous section, the stationary propagation corresponds to a constant crack propagation rate. This regime will

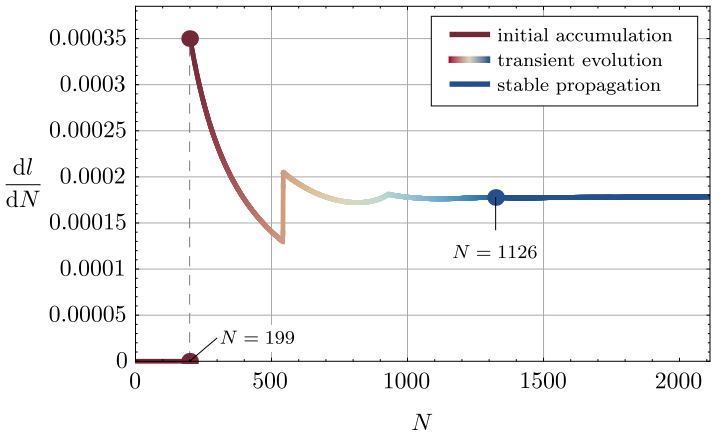

Fig. 11. Crack propagation rate with respect to the number of cycles. The discontinuity at $N \approx 540$ is reflected by the slope discontinuity at $l = \ell_f$ of the fatigue history variable profile in Fig. 12.

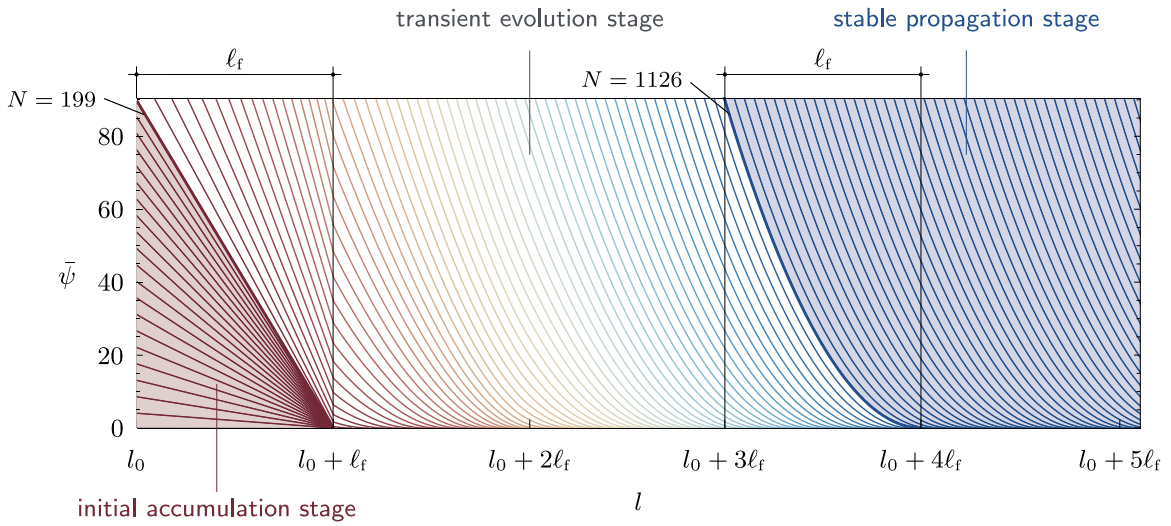

Fig. 12. Fatigue history variable evolution, with profiles plotted every 20 cycles, and highlight of the three evolution stages. Before crack propagation is triggered, the fatigue history variable profile is linear. Once the crack starts to propagate, the profile tends to a parabolic shape, constant during the stable propagation stage. Each profile vanishes at distances greater than ℓ_f from the crack tip. The discontinuity in the slope profile at $l = \ell_f$ is reflected by the discontinuity at $N \approx 540$ in the crack rate plot of Fig. 11.

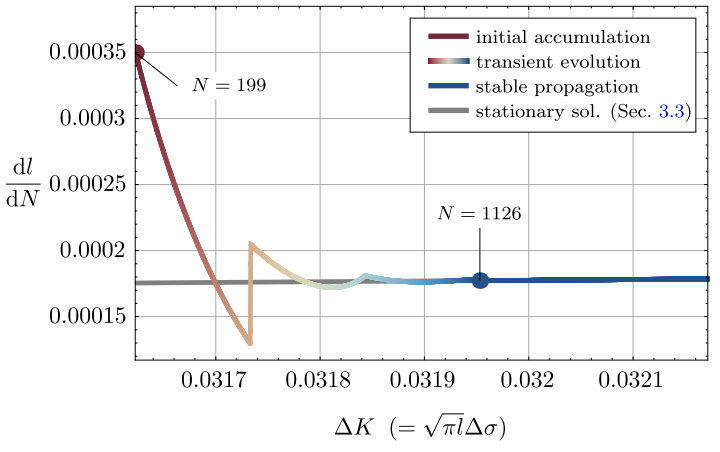

Fig. 13. Crack propagation rate with respect to the stress intensity factor variation.

Table 2
The distinguishing features of the fatigue models considered for the stationary fatigue crack propagation regime.

Model	Fatigue functions		Result type	Features
	g_3	g_4		
①	1	1	analytical in closed form	Paris' law with exponent 1
②	$\tilde{\psi}$	1	analytical in closed form	Paris' law with exponent 1 and mean load effect
③	1	$\left(\psi^*({}^t\bar{\psi})\right)^q$	analytical/numerical	Paris' law with variable slope/exponent

allow us to derive, for instance, a rigorous link between the present model and Paris' law, and to understand the role played by the functions g_3 and g_4 in the fatigue crack evolution.

The IPSC setup is again considered under mode-I loading conditions. Differently from the previous section, simple tension–tension K-cyclic loadings are now assumed whilst the initial accumulation and the transient evolution stages are neglected. As in the previous section, we consider a linear threshold function, a linear fatigue function, and a FDZ significantly smaller than the KDZ, namely:

$$h(r) = h_1(r), \tag{51a}$$

$$f(\phi) = f_1(\phi), \tag{51b}$$

$$\ell_{\mathrm{f}} \ll \ell_{\mathrm{k}}, \tag{51c}$$

but different expressions for the fatigue history variable (28). The resulting models investigated in this section are listed in Table 2. The assumption (51a) renders the fatigue propagation independent of the far field elastic energy density. Accordingly, it is reasonable to consider only the linear fatigue degradation function, namely, (51b), since the far field fatigue history variable vanishes. These choices will be crucial to derive simple closed form results for the stationary propagation stage. The assumption (51c) allows us to consider only the singular part of the elastic energy density (A.9).

3.3.1. The stationary regime setting

The stationary regime is characterized by the following assumptions:

$$\Delta l_i = \Delta l, \tag{52a}$$

$$\Delta K_i = \Delta K, \tag{52b}$$

$$\Delta l \ll \ell_{\mathrm{f}}, \tag{52c}$$

$$\ell_{\mathrm{f}} \bmod \Delta l = 0 \quad \text{with} \quad \frac{\ell_{\mathrm{f}}}{\Delta l} = N_{\mathrm{f}}. \tag{52d}$$

The index i refers to the cycle number according to the notation of Fig. 9. Assumption (52a) represents the essential feature of the stationary response, that is, a constant crack length advancement at each load cycle. The crack propagation rate with respect to the load cycles can then be directly identified with the crack length increment, namely:

$$\Delta l \approx \frac{\mathrm{d}\, l}{\mathrm{d}N}. \tag{53}$$

Conditions (51c), (52b), (52c) and (52d) allow us to obtain the stationary response. Specifically, they lead to a fatigue variable evolution which is crack length independent, with the shape of the elastic energy density field ahead of the crack tip always the same within the KDZ. Indeed, the elastic energy density on the crack path at a peak load can be approximated by (A.9), that is, in the local reference by

$$\psi(t, r) \approx k_\psi \frac{K(t)^2}{r}, \tag{54}$$

with $k_\psi = \frac{(1-\nu)}{2E\pi}$ (for plane-stress). Moreover, to guarantee a cycle-independent stress intensity factor variation (ΔK = constant), the far field stress becomes a fracture length dependent quantity, namely,

$$\sigma(l) = K/\sqrt{l\pi}. \tag{55}$$

Condition (52d), together with (51a), will allow us to take advantage of recursive expressions to derive the fatigue variable evolution in closed form. This will be the computational key to easily derive the fatigue crack law for the description of the stationary propagation regime.

3.3.2. Stationary evolution stages and fatigue variable

In this section, the fatigue variable (27) is first explicitly computed for all models considered in Table 2. Specifically, we derive closed form expressions for $\bar{\psi}_N(r = 0)$, that is, the value of the fatigue history variable at cycle N at the crack tip ($r = 0$), and for $\bar{\psi}_0$, that is, the critical value of the fatigue history variable for monotonic loading. Before facing these computations, it is important to understand the different stages of the stationary evolution within a single load cycle in relation to the elastic energy density profile. Specifically, we identify the following cycle stages:

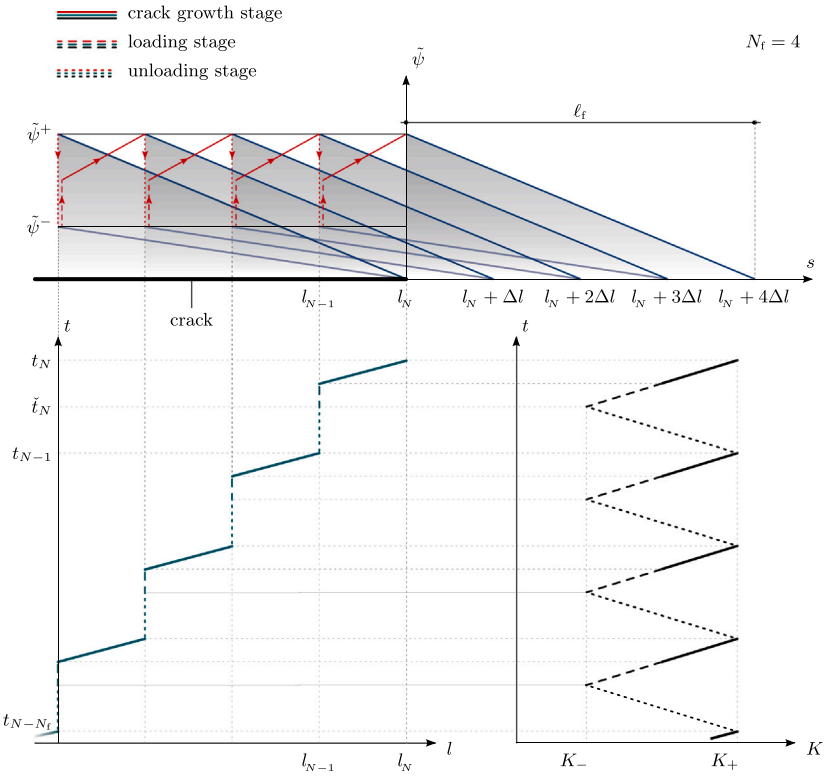

Fig. 14. Paradigmatic evolutions of the smoothed energy $\tilde{\psi}$, the crack length l, and the loading in terms of the stress intensity factor K for $N_f = 4$. The evolution, loading and unloading stages are emphasized with different line styles. Of course, the evolution of l is represented as a piecewise-linear function only for illustration purposes.

- the *loading stage*, ($\dot{l} = 0$ and $\dot{\tilde{\psi}} \neq 0$);
- the *crack growth stage* ($\dot{l} \neq 0$);
- the *unloading stage*, ($\dot{l} = 0$ and $\dot{\tilde{\psi}} = 0$).

The evolution of the smoothed energy $\tilde{\psi}$, the crack length l, and the loading in terms of the stress intensity factor K are highlighted in Fig. 14 with respect to these stages for a time-interval of the stationary fatigue crack response. According to the assumptions (51) and the expression of the elastic energy density (54), the smoothed energy reads

$$\tilde{\psi}(r) = g_1(r,\psi) = h_1(r)\sqrt{r}\sqrt{\psi(r)} = \begin{cases} \dfrac{k_h\sqrt{k_\psi}}{\ell_f}\left(1 - \dfrac{r}{\ell_f}\right) K, & \text{if } 0 \le r \le \ell_f, \\ 0, & \text{if } r > \ell_f, \end{cases} \tag{56}$$

corresponding to a linear function, starting form the crack tip, decreasing to zero as $r \to \ell_f$ and proportional to the stress intensity factor. Hereafter, the evolution of the fatigue variable for each model considered in Table 2 is derived, based on the evolution of the smoothed energy $\tilde{\psi}$ defined in (56) and depicted in Fig. 14.

Model ①. For this model, the fatigue history variable is defined as follows:

$$\bar{\psi}_N(r) = \int_0^{t_N} \left(\dot{\tilde{\psi}}(\tau, r)\right)^+ \mathrm{d}\tau, \tag{57}$$

where $\square_N$ denotes that the quantity $\square$ has been computed up to the Nth cycle, corresponding to the time instant t_N. The positive rate extracted by $(\square)^+$ ensures that accumulation occurs during loading stages only, that is, from $\check{t}_i$ only. Note that the fatigue history variable can be seen as a sum of single contributions.

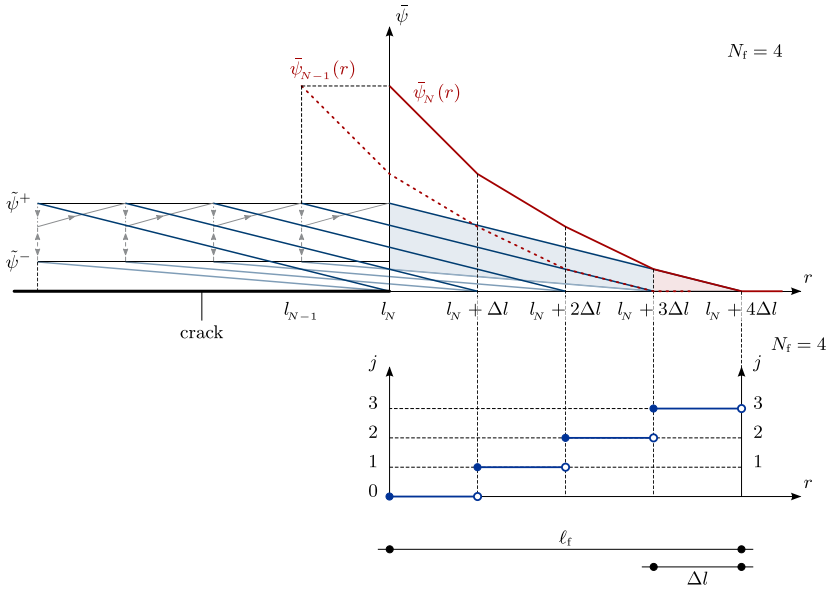

Fig. 15. Fatigue variable profile evolution for model ① according to Fig. 14 and definition of the adopted notation.

In view of (56), the fatigue history variable increment is constant for each cycle and given by

$$\Delta\bar{\psi} = \begin{cases} \dfrac{k_h\sqrt{k_\psi}}{\ell_f}\left(\left(1-\dfrac{r}{\ell_f}\right)K_+ - \left(1-\dfrac{r+\Delta l}{\ell_f}\right)K_-\right), & \text{if } 0 \le r \le \ell_f - \Delta l, \quad \text{(a)} \\ \dfrac{k_h\sqrt{k_\psi}}{\ell_f}\left(1-\dfrac{r}{\ell_f}\right)K_+, & \text{if } \ell_f - \Delta l < r \le \ell_f, \quad \text{(b)} \\ 0, & \text{if } r > \ell_f\,. \quad \text{(c)} \end{cases} \tag{58}$$

These single contributions are highlighted in Fig. 15. Specifically, (58a) corresponds to the blue region, as the result of the difference of two extreme values, whereas (58b) corresponds to the red region where only the last upper energy profile contributes to $\Delta\bar{\psi}$. Due to the adoption of the linear fatigue threshold function, no fatigue history variable increment occurs for $r \ge \ell_f$.

Inferring the result in (58), that is, by considering all the contributions to the fatigue variable for each load cycle, and considering the notation in Fig. 15, the fatigue variable associated to a crack propagated up to length l_N corresponding to the Nth cycle is given by

$$\begin{aligned} \bar{\psi}_N(r) &= \int_0^{t_N} \left(\dot{\bar{\psi}}(\tau, r)\right)^+ \mathrm{d}\tau \\ &= \int_{t_{N-N_f}}^{t_N} \left(\dot{\bar{\psi}}(\tau, r)\right)^+ \mathrm{d}\tau \\ &= \sum_{i=1}^{N_f} \Delta\bar{\psi}_i \\ &= \frac{k_h\sqrt{k_\psi}}{\ell_f}\left(\sum_{i=0}^{N_f-1-j}\left(1-\frac{r+i\,\Delta l}{\ell_f}\right)K_+ - \sum_{i=1}^{N_f-1-j}\left(1-\frac{r+i\,\Delta l}{\ell_f}\right)K_-\right), \end{aligned} \tag{59}$$

with $j = \left\lfloor \frac{r}{\Delta l} \right\rfloor$, $\Delta\bar{\psi}_i$ referring to a fatigue history variable increment (58) of a crack propagated up to l_i, and $\sum_{i=a}^{b} \square_i = 0$ if $b < a$. This fatigue history variable profile, represented by a red solid curve in Fig. 15, consists of a piecewise continuous linear function.

Since we are interested in the crack propagation conditions (21), it is important to evaluate the value of the fatigue variable at the crack tip. Recalling the assumption (52c), the result (59), and noting that $\sum_{i=1}^{N} i = \frac{1}{2}N(N+1)$, the fatigue history variable at

the crack tip reads

$$\begin{aligned}\bar{\psi}_N(0) &= \frac{k_\mathrm{h}\sqrt{k_\psi}}{\ell_\mathrm{f}}\left(\left(N_\mathrm{f}-1\right)\left(1-\frac{\Delta l}{2\ell_\mathrm{f}}N_\mathrm{f}\right)\Delta K + K_+\right)\\ &= \frac{k_\mathrm{h}\sqrt{k_\psi}}{\ell_\mathrm{f}}\left(\frac{1}{2}\left(\frac{\ell_\mathrm{f}}{\Delta l}-1\right)\Delta K + K_+\right)\\ &\approx \frac{k_\mathrm{h}\sqrt{k_\psi}}{\ell_\mathrm{f}}\left(\frac{1}{2}\frac{\ell_\mathrm{f}}{\Delta l}\Delta K + \bar{K}\right),\end{aligned} \tag{60}$$

in terms of the variation and mean value of the stress intensity factor.

To establish the fatigue crack propagation law, the fatigue variable value $\bar{\psi}_0$ at the monotonic fracture limit must be evaluated. In view of (45), we have

$$\bar{\psi}_0 = \frac{k_\mathrm{h}\sqrt{k_\psi}}{\ell_\mathrm{f}}\sqrt{\frac{G_\mathrm{c}}{k_\mathrm{G}}}. \tag{61}$$

Expressions (60) and (61) will be employed in Section 3.3.3 to derive the fatigue crack propagation law in closed form.

Model ②. For this model, the fatigue history variable is defined as follows:

$$\bar{\psi}_{_N}(r) = \int_0^{t_N}\left(\tilde{\psi}(\tau,r)\,\dot{\tilde{\psi}}(\tau,r)\right)^+\mathrm{d}\tau = \frac{1}{2}\int_0^{t_N}\left(\frac{\mathrm{d}}{\mathrm{d}\tau}\left(\tilde{\psi}(\tau,r)^2\right)\right)^+\mathrm{d}\tau. \tag{62}$$

According to Table 2 and in view of (56), the fatigue history variable increment is also constant for each cycle in this model and given by

$$\Delta\bar{\psi} = \begin{cases}\dfrac{k_\mathrm{h}^2 k_\psi}{2\ell_\mathrm{f}^2}\left(\left(1-\dfrac{r}{\ell_\mathrm{f}}\right)^2 K_+^2 - \left(1-\dfrac{r+\Delta l}{\ell_\mathrm{f}}\right)^2 K_-^2\right), & \text{if } 0\le r\le \ell_\mathrm{f}-\Delta l,\\ \dfrac{k_\mathrm{h}^2 k_\psi}{2\ell_\mathrm{f}^2}\left(1-\dfrac{r}{\ell_\mathrm{f}}\right)^2 K_+^2, & \text{if } \ell_\mathrm{f}-\Delta l < r\le \ell_\mathrm{f},\\ 0, & \text{if } r>\ell_\mathrm{f}.\end{cases} \tag{63}$$

Inferring the result in (63), that is, by considering all the contributions to the fatigue variable for each load cycle, and considering again the notation in Fig. 15, the fatigue variable associated to a crack propagated up to length $l_{_N}$ corresponding to the Nth cycle is given by

$$\begin{aligned}\bar{\psi}_{_N}(r) &= \frac{1}{2}\int_0^{t_N}\left(\frac{\mathrm{d}}{\mathrm{d}\tau}\left(\tilde{\psi}(\tau,r)^2\right)\right)^+\mathrm{d}\tau\\ &= \frac{1}{2}\int_{t_{N-N_\mathrm{f}}}^{t_N}\left(\frac{\mathrm{d}}{\mathrm{d}\tau}\left(\tilde{\psi}(\tau,r)^2\right)\right)^+\mathrm{d}\tau\\ &= \sum_{i=1}^{N_\mathrm{f}}\Delta\bar{\psi}_i\\ &= \frac{k_\mathrm{h}^2 k_\psi}{2\ell_\mathrm{f}^2}\left(\sum_{i=0}^{N_\mathrm{f}-1-j}\left(1-\frac{r+i\,\Delta l}{\ell_\mathrm{f}}\right)^2 K_+^2 - \sum_{i=1}^{N_\mathrm{f}-1-j}\left(1-\frac{r+i\,\Delta l}{\ell_\mathrm{f}}\right)^2 K_-^2\right)\\ &= \frac{k_\mathrm{h}^2 k_\psi}{2\ell_\mathrm{f}^2}\left(\sum_{i=1}^{N_\mathrm{f}-1-j}\left(1-\frac{r+i\,\Delta l}{\ell_\mathrm{f}}\right)^2\left(K_+^2-K_-^2\right) + \left(1-\frac{r}{\ell_\mathrm{f}}\right)^2 K_+^2\right).\end{aligned} \tag{64}$$

Differently from model ①, the fatigue history variable profile now consists of a piecewise continuous quadratic function.

Recalling that $\sum_{i=1}^{N} i = \frac{1}{2}N(N+1)$, $\sum_{i=1}^{N} i^2 = \frac{1}{6}N(N+1)(2N+1)$, $\left(K_+^2-K_-^2\right) = 2\bar{K}\Delta K$, and with similar considerations done in (59), the fatigue variable at the crack tip reads

$$\begin{aligned}\bar{\psi}_N(0) &= \frac{k_\mathrm{h}^2 k_\psi}{2\ell_\mathrm{f}^2}\left(2\bar{K}\Delta K\sum_{i=1}^{N_\mathrm{f}-1}\left(1-\frac{i\,\Delta l}{\ell_\mathrm{f}}\right)^2 + K_+^2\right)\\ &= \frac{k_\mathrm{h}^2 k_\psi}{2\ell_\mathrm{f}^2}\left(2\bar{K}\Delta K\sum_{i=1}^{N_\mathrm{f}-1}\left(1-2\frac{\Delta l}{\ell_\mathrm{f}}i+\frac{\Delta l^2}{\ell_\mathrm{f}^2}i^2\right) + K_+^2\right)\\ &= \frac{k_\mathrm{h}^2 k_\psi}{2\ell_\mathrm{f}^2}\left(\frac{1}{3}\bar{K}\Delta K\left(\frac{N_\mathrm{f}-1}{N_\mathrm{f}}\right)\left(2N_\mathrm{f}-1\right) + K_+^2\right),\end{aligned} \tag{65}$$

in terms of the variation, mean value, and maximum value of the stress intensity factor. Due to the assumption (52c), that is, $N_\mathrm{f}\gg 1$,

$$\left(\frac{N_\mathrm{f}-1}{N_\mathrm{f}}\right)\left(2N_\mathrm{f}-1\right)\approx 2N_\mathrm{f}. \tag{66}$$

As a consequence, (65) can be approximated as follows:

$$\bar{\psi}_N(0) \approx \frac{k_{\mathrm{h}}^2 k_\psi}{2\ell_{\mathrm{f}}^2}\left(\frac{2}{3}N_{\mathrm{f}}\bar{K}\Delta K + K_+^2\right) = \frac{k_{\mathrm{h}}^2 k_\psi}{2\ell_{\mathrm{f}}^2}\left(\frac{2}{3}\frac{\ell_{\mathrm{f}}\bar{K}\Delta K}{\Delta l} + K_+^2\right). \tag{67}$$

For the present model, the fatigue variable $\bar{\psi}_0$ at the monotonic fracture limit reads

$$\bar{\psi}_0 = \frac{k_{\mathrm{h}}^2 k_\psi}{2\ell_{\mathrm{f}}^2}\frac{G_{\mathrm{c}}}{k_{\mathrm{G}}}. \tag{68}$$

Expressions (67) and (68) will be employed in Section 3.3.3 to derive the fatigue crack propagation law in closed form.

Model ③. For this last model, the fatigue history variable is defined as follows:

$$\bar{\psi}_N(r) = \int_0^{t_N}\left(\psi^*({}^t\bar{\psi})\right)^q\left(\dot{\bar{\psi}}\right)^+\mathrm{d}\tau. \tag{69}$$

As done for the previous models, let us evaluate the fatigue variable increment for a generic load cycle. According to Table 2, and in view of (56), we have

$$\begin{aligned}
\Delta\bar{\psi} &= \int_{\check{t}_N}^{t_N}\left(\int_{\check{t}_N}^{\tau}\dot{\bar{\psi}}(\tilde{\tau},r)\,\mathrm{d}\tilde{\tau}\right)^q\dot{\bar{\psi}}(\tau,r)\,\mathrm{d}\tau\\
&= \frac{1}{q+1}\int_{\check{t}_N}^{t_N}\frac{\mathrm{d}}{\mathrm{d}\tau}\left(\int_{\check{t}_N}^{\tau}\dot{\bar{\psi}}(\tilde{\tau},r)\,\mathrm{d}\tilde{\tau}\right)^{q+1}\mathrm{d}\tau\\
&= \frac{1}{q+1}\left(\int_{\check{t}_N}^{t_N}\dot{\bar{\psi}}(\tilde{\tau},r)\,\mathrm{d}\tilde{\tau}\right)^{q+1}\\
&= \begin{cases}
\dfrac{1}{q+1}\left(\dfrac{k_{\mathrm{h}}\sqrt{k_\psi}}{\ell_{\mathrm{f}}}\left(\left(1-\dfrac{r}{\ell_{\mathrm{f}}}\right)K_+ - \left(1-\dfrac{r+\Delta l}{\ell_{\mathrm{f}}}\right)K_-\right)\right)^{q+1}, & \text{if } 0\le r\le \ell_{\mathrm{f}}-\Delta l,\\
\dfrac{1}{q+1}\left(\dfrac{k_{\mathrm{h}}\sqrt{k_\psi}}{\ell_{\mathrm{f}}}\left(1-\dfrac{r}{\ell_{\mathrm{f}}}\right)K_+\right)^{q+1}, & \text{if } \ell_{\mathrm{f}}-\Delta l< r\le \ell_{\mathrm{f}},\\
0, & \text{if } r>\ell_{\mathrm{f}}.
\end{cases}
\end{aligned} \tag{70}$$

The fatigue history variable then reads

$$\bar{\psi}_N(r) = \frac{1}{q+1}\left(\frac{k_{\mathrm{h}}\sqrt{k_\psi}}{\ell_{\mathrm{f}}}\right)^{q+1}\left(\sum_{i=0}^{N_{\mathrm{f}}-2-j}\left(\left(1-\frac{r+i\,\Delta l}{\ell_{\mathrm{f}}}\right)\Delta K + \frac{\Delta l}{\ell_{\mathrm{f}}}K_-\right)^{q+1} + \left(\left(1-\frac{r+(N_{\mathrm{f}}-1)\,\Delta l}{\ell_{\mathrm{f}}}\right)K_+\right)^{q+1}\right). \tag{71}$$

The fatigue variable at the crack tip reads

$$\bar{\psi}_N(0) = \frac{1}{q+1}\left(\frac{k_{\mathrm{h}}\sqrt{k_\psi}}{\ell_{\mathrm{f}}}\right)^{q+1}\left(\sum_{i=0}^{N_{\mathrm{f}}-2}\left(\left(1-\frac{i\,\Delta l}{\ell_{\mathrm{f}}}\right)\Delta K + \frac{\Delta l}{\ell_{\mathrm{f}}}K_-\right)^{q+1} + \left(\frac{1}{N_{\mathrm{f}}}K_+\right)^{q+1}\right). \tag{72}$$

Unfortunately, we have not found more compact expressions for Eqs. (71) and (72).

For the present model, the fatigue variable $\bar{\psi}_0$ at the monotonic fracture limit reads

$$\bar{\psi}_0 = \left(\frac{1}{q+1}\right)\left(\frac{k_{\mathrm{h}}\sqrt{k_\psi}}{\ell_{\mathrm{f}}}\sqrt{\frac{G_{\mathrm{c}}}{k_{\mathrm{G}}}}\right)^{q+1}. \tag{73}$$

Expressions (72) and (73) will be employed in Section 3.3.3 to derive the fatigue crack propagation law.

3.3.3. The fatigue crack propagation law

In this section, the fatigue crack propagation law of each model considered in Table 2 is derived and discussed based on the fatigue variable expressions derived in the previous section (Section 3.3.2).

The general strategy to derive the fatigue crack propagation law is to consider the end of a load cycle, where the crack evolution conditions are met. Specifically, in view of (7), (19) and (21), we have

$$G = G_{\mathrm{f}}(\phi(l)) \qquad \rightarrow \qquad k_{\mathrm{G}}K_+^2 = \left(1+k_{\mathrm{f}}\left(1-\frac{\bar{\psi}_N(0)}{\bar{\psi}_0}\right)\right)G_{\mathrm{c}}. \tag{74}$$

Model ①*: Paris' law with exponent 1.* By injecting (60) and (61) into (74) we obtain

$$\begin{aligned}
k_{\mathrm{G}}K_+^2 &= \left(1+k_{\mathrm{f}}\left(1-\sqrt{\frac{k_{\mathrm{G}}}{G_{\mathrm{c}}}}\left(\frac{1}{2}\frac{\ell_{\mathrm{f}}}{\Delta l}\Delta K + \bar{K}\right)\right)\right)G_{\mathrm{c}}\\
&= G_{\mathrm{c}}(1+k_{\mathrm{f}}) - k_{\mathrm{f}}\sqrt{k_{\mathrm{G}}G_{\mathrm{c}}}\bar{K} - \frac{k_{\mathrm{f}}\ell_{\mathrm{f}}\sqrt{k_{\mathrm{G}}G_{\mathrm{c}}}}{2}\frac{\Delta K}{\Delta l},
\end{aligned} \tag{75}$$

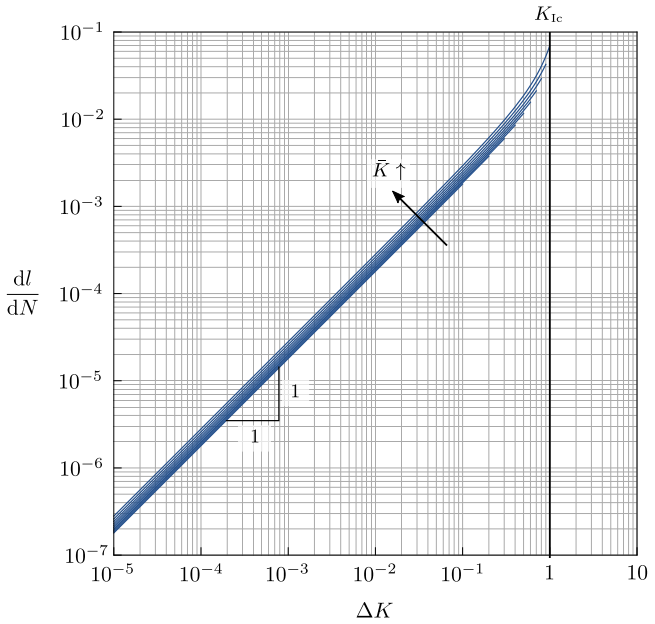

Fig. 16. Representation of (76) for different values of $\bar{K}$ ranging from 0.05 to 0.5 with a step of 0.05. The PR corresponds to Paris' law with exponent 1 and a weak depedence on $\bar{K}$.

from which, in view of (53), the crack propagation rate as a function of the stress intensity factor variation is obtained:

$$\begin{aligned}\frac{\mathrm{d}\,l}{\mathrm{d}N} &= \frac{1}{2}\left(\frac{k_{\mathrm{f}}\ell_{\mathrm{f}}\sqrt{k_{\mathrm{G}}G_{\mathrm{c}}}}{G_{\mathrm{c}}(1+k_{\mathrm{f}}) - k_{\mathrm{f}}\sqrt{k_{\mathrm{G}}G_{\mathrm{c}}}\bar{K} - k_{\mathrm{G}}K_{+}^{2}}\right)\Delta K \\ &= \frac{1}{2}\left(\frac{k_{\mathrm{f}}\ell_{\mathrm{f}}\sqrt{k_{\mathrm{G}}G_{\mathrm{c}}}}{\left(G_{\mathrm{c}} - k_{\mathrm{G}}K_{+}^{2}\right) + k_{\mathrm{f}}\left(G_{\mathrm{c}} - \sqrt{k_{\mathrm{G}}G_{\mathrm{c}}}\bar{K}\right)}\right)\Delta K.\end{aligned} \tag{76}$$

The following remarks can be drawn form this expression:

- (76) does not depend on k_{h} since the fatigue variable is normalized with respect to its monotonic value, but it does depend on the fatigue length ℓ_{f};
- (76) is very close to the expression of Paris' law (12), namely:

$$\frac{\mathrm{d}\,l}{\mathrm{d}N} = C(K_{+},\bar{K})\Delta K, \tag{77}$$

  with Paris' exponent $m = 1$ and the Paris' coefficient weakly depending on K_{+} and $\bar{K}$;
- we observe two meaningful limit cases of (76):
  - if $K_{+}/K_{\mathrm{Ic}} \to 0$ and in view of (7), $C(K_{+},\bar{K}) \to C$, namely:

$$\frac{\mathrm{d}\,l}{\mathrm{d}N} = C\,\Delta K \qquad \text{with} \qquad C = \left(\frac{k_{\mathrm{f}}\ell_{\mathrm{f}}\sqrt{k_{\mathrm{G}}}}{2\left(1+k_{\mathrm{f}}\right)\sqrt{G_{\mathrm{c}}}}\right), \tag{78}$$

    which is Paris' law (12) with exponent $m = 1$.
  - if $\Delta K \to K_{\mathrm{Ic}}$, implying that $K_{+} \to K_{\mathrm{Ic}}$ and $\bar{K} \to K_{\mathrm{Ic}}/2$, that is, the stress intensity approaches the maximum allowable value, $C(K_{+},\bar{K})$ tends to a maximum but finite value and, therefore, the fatigue crack propagation rate tends to be maximal.

  These results suggest that this very simple model is already capable of describing both the Paris' regime (PR) and, albeit less accurately, the fast crack growth regime (FR).

The above mentioned results can be observed in Fig. 16, where the trend of the fatigue crack propagation law (76) is represented for different values of the mean stress intensity factor. Here, the initial crack length has been chosen as $l_0 = 10$, the fatigue length as $\ell_{\mathrm{f}} = 0.007 l_0$ ($\approx 1/10\,\ell_{\mathrm{k}}$), and all other constants are of unitary value, except for Poisson's ratio ($\nu = 0.25$).

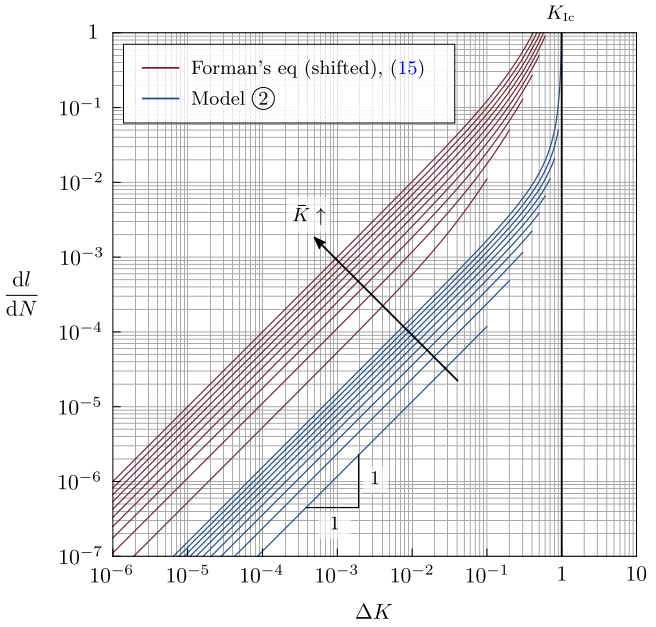

Fig. 17. Mean load effect as a function of $\bar{K}$, ranging from 0.05 to 0.5 with a step of 0.05. The PR is described by Paris' law with exponent 1 and a strong dependence on $\bar{K}$. Blue curves correspond to the model crack propagation curve (80) whereas red curves correspond to Forman's Eq. (15), shifted upwards for graphical reasons in order to avoid confusing overlaps.

Model ②: Paris' law with exponent 1 and mean load effect. By injecting (67) and (68) into (74) we obtain

$$\begin{aligned} k_{\mathrm{G}}K_+^2 &= \left(1+k_{\mathrm{f}}\left(1-\frac{k_{\mathrm{G}}}{G_{\mathrm{c}}}\left(\frac{2}{3}\frac{\ell_{\mathrm{f}}\bar{K}\Delta K}{\Delta l}+K_+^2\right)\right)\right)G_{\mathrm{c}} \\ &= G_{\mathrm{c}}(1+k_{\mathrm{f}})-\frac{2}{3}k_{\mathrm{f}}k_{\mathrm{G}}\ell_{\mathrm{f}}\bar{K}\frac{\Delta K}{\Delta l}-k_{\mathrm{f}}k_{\mathrm{G}}K_+^2, \end{aligned} \tag{79}$$

from which, in view of (53), the crack propagation rate as a function of the stress intensity factor variation is obtained:

$$\begin{aligned} \frac{\mathrm{d}l}{\mathrm{d}N} &= \frac{2}{3}\left(\frac{k_{\mathrm{f}}k_{\mathrm{G}}\ell_{\mathrm{f}}\bar{K}}{G_{\mathrm{c}}(1+k_{\mathrm{f}})-k_{\mathrm{G}}(1+k_{\mathrm{f}})K_+^2}\right)\Delta K \\ &= \frac{2}{3}\left(\frac{k_{\mathrm{f}}k_{\mathrm{G}}\ell_{\mathrm{f}}\bar{K}}{(1+k_{\mathrm{f}})(G_{\mathrm{c}}-k_{\mathrm{G}}K_+^2)}\right)\Delta K. \end{aligned} \tag{80}$$

The following remarks can be drawn form (80):

- as in (76), (80) does not depend on k_{h};
- (80) is again very close to the expression of Paris' law (12), namely,

$$\frac{\mathrm{d}l}{\mathrm{d}N} = C(K_+,\bar{K})\,\Delta K, \tag{81}$$

  with Paris' coefficient $m = 1$. Nevertheless, in this case, the Paris' coefficient depends strongly on $\bar{K}$ but weakly on K_+. If $K_+/K_{\mathrm{Ic}} \to 0$, C tends to become linear with respect to $\bar{K}$, as highlighted by the following remark where limit cases are discussed;
- we observe two meaningful limit cases of (80):
  - if $K_+ \ll K_{\mathrm{Ic}}$ and in view of (7), $C(K_+,\bar{K}) \to C\bar{K}$, namely:

$$\frac{\mathrm{d}l}{\mathrm{d}N} = C\bar{K}\,\Delta K, \qquad \text{with} \qquad C=\frac{2k_{\mathrm{f}}k_{\mathrm{G}}\ell_{\mathrm{f}}}{3(1+k_{\mathrm{f}})G_{\mathrm{c}}}, \tag{82}$$

    which corresponds to Paris' law (12) with exponent 1 but a linear dependence on the mean value of the stress intensity factor. Expression (82) is similar but not equal to (15). However, both appear to describe the same behavior;
  - if $\Delta K \to K_{\mathrm{Ic}}$, implying that $K_+ \to K_{\mathrm{Ic}}$, that is, the stress intensity approaches the maximum allowable value, $C(K_+,\bar{K}) \to \infty$ and the fatigue crack propagation rate tends to infinity.

These results suggest that this very simple model is already capable of describing both the Paris' regime (PR), the fast crack growth regime (FR), and a linear dependence on the mean value of the stress intensity factor.

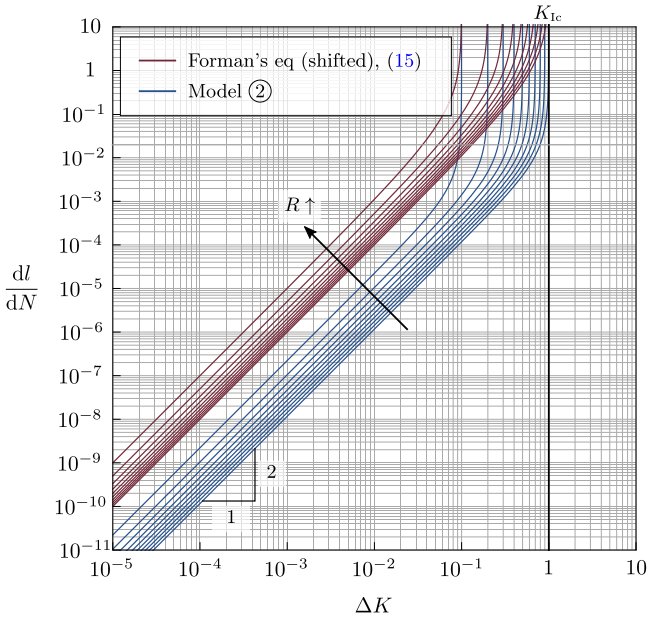

Fig. 18. Mean load effect as a function of R, ranging from 0 to 0.9 with a step of 0.1. The PR is described by Paris' law with exponent 2 and a strong dependence on R. Blue curves correspond to the model crack propagation curve (80) whereas red curves correspond to Forman's Eq. (13), shifted upwards for graphical reasons in order to avoid confusing overlaps.

The above mentioned results can be observed in Fig. 17 and Fig. 18, where the trend of the fatigue crack propagation law (80) is presented for different values of mean stress intensity factor $\bar{K}$ and the load parameter R, respectively. The same numerical values of the previous examples have been adopted for the material constants. Surprisingly, the response exhibited by the model is very similar to the empirical one suggested by Forman, *i.e.*, Eq. (15).

Model ③: Paris' law with variable exponent/slope. For this model, it has been impossible to evaluate the summation (72) in a closed form. Therefore, no analytical expression for the fatigue crack propagation law is provided. Nevertheless, the problem has been faced numerically. Specifically, different crack propagation rates Δl have been prescribed and the corresponding stress intensity factor variations have been obtained by solving the non-linear problem (74). Different values for the exponent q in (43) have been considered and the outcomes are presented in Fig. 19.

What is immediately evident from these results is that the Paris' exponent m is linked to the exponent q of (43) by the following relation:

$$m \approx q + 1. \tag{83}$$

This result can also be intuitively understood by looking closer to (72). Indeed, it is exactly $q+1$ that raises ΔK to power while the summation yields a linear function of $\ell_{\mathrm{f}}/\Delta l$ in (74).

These results clearly highlight the role played by (43) and in particular by ψ^* in being able to tune the slope of the fatigue crack propagation curve in the Paris' regime.

3.4. The case of a FDZ greater than the KDZ and linear/exponential threshold function comparison

In this section, the occurrence of a fatigue zone greater than the K-dominance zone is considered, for which knowledge of the exact elastic solution of the problem turns out to be of fundamental importance. At the same time, the effects of adopting a linear or exponential threshold function are compared.

Within a plane-stress setting, the IPSC setup is again considered under mode-I loading conditions. Differently from the previous section, a simple tension–tension σ-cyclic loading is now assumed, with $\sigma_- = 0$ and $\sigma_+ = 0.01\sigma_0$, where $\sigma_0 := K_{\mathrm{Ic}}/\sqrt{\pi l_0}$ corresponds to the limit far field stress for a monotonic load. Consequently, $\Delta\sigma = 0.01\sigma_0$ and $R = 0$. In addition, the assumed initial crack length and K-dominance length are $l_0 = 10$ and $\ell_{\mathrm{k}} = 0.07 l_0$, respectively, whereas different fatigue lengths were considered, specifically, $\ell_{\mathrm{f}} \in \{1, 5, 25\} \times \ell_{\mathrm{k}}$. All the analyses are done with model ① of Table 2. The remainder of the constitutive constants have been chosen of unitary value, except for Poisson's ratio ($\nu = 0.25$).

For the discussion of the subsequent results, it is preliminarily useful to highlight the elastic energy profiles of both the K-solution (A.9) and the exact solution (A.8). These are represented in Fig. 20, normalized with respect to the value of the K-solution evaluated at $r = l_0$, namely:

$$\hat{\psi} = \frac{K_{\mathrm{I}}^2(1-\nu)}{2\pi E}. \tag{84}$$

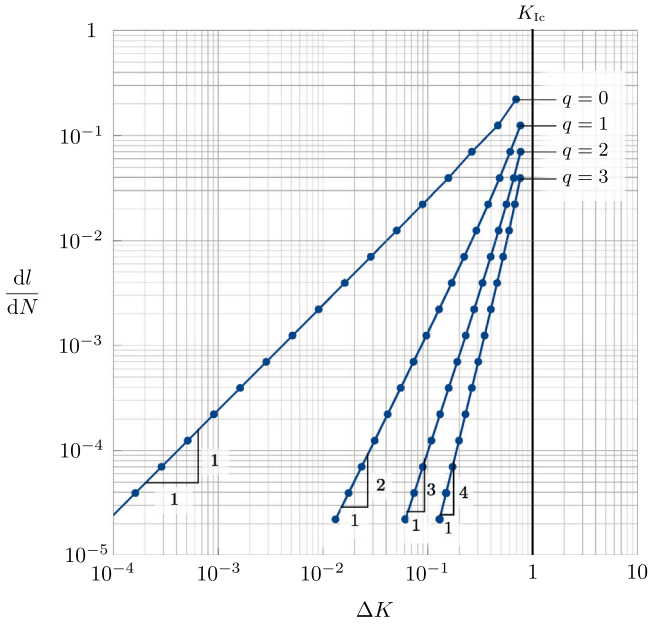

Fig. 19. Stable crack propagation laws for different values of $q \in \{0, 1, 2, 3\}$ corresponding respectively to Paris' law exponents $m \in \{1, 2, 3, 4\}$.

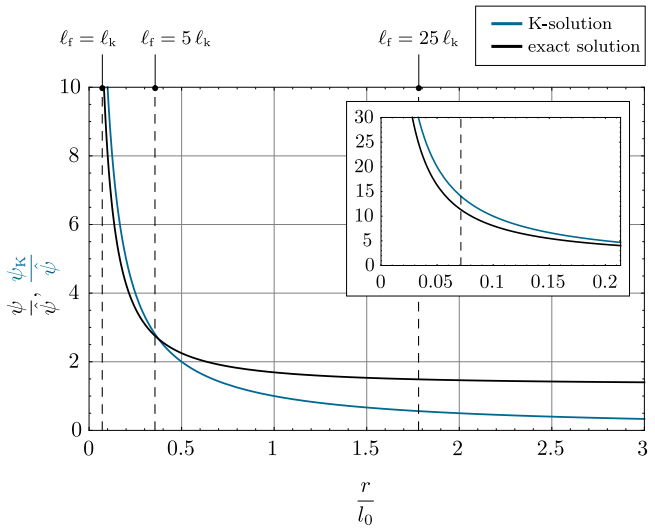

Fig. 20. Elastic energy profiles of the K-solution (A.9) and the exact solution (A.8).

Along the crack path, the elastic energy density of the K-solution is clearly underestimated far from the crack tip compared to the elastic energy density of the exact solution, since the former tends to vanish whereas the latter tends to the far field stress value. However, interestingly, the elastic energy is higher for the K-solution close to the crack tip. For the present example, this trend inversion is approximately observed at $\ell_{\mathrm{f}} = 5\ell_{\mathrm{k}}$.

The fatigue history variable profiles with respect to the load cycles are reported in Fig. 21 for different values of $\ell_{\mathrm{f}}/\ell_{\mathrm{k}}$ and for different threshold functions. The corresponding crack and crack rate evolutions with respect to the number of cycles are displayed in Figs. 22 and 23 for both the linear and exponential threshold functions. Finally, the crack rate evolutions with respect to the stress intensity factor variation and again for both threshold functions are highlighted in Figs. 24 and 25.

For $\ell_{\mathrm{f}}/\ell_{\mathrm{k}}$ equal to 1 and 5, the fatigue history variable profiles are quite similar to each other for both the linear and exponential threshold functions. Nevertheless, the transient evolution region is much wider with h_{l}, approximately three times the fatigue length in the present case, as also observed in Fig. 12, whereas with h_{e}, the same region is only a fraction of ℓ_{f}. Clearly, by adopting

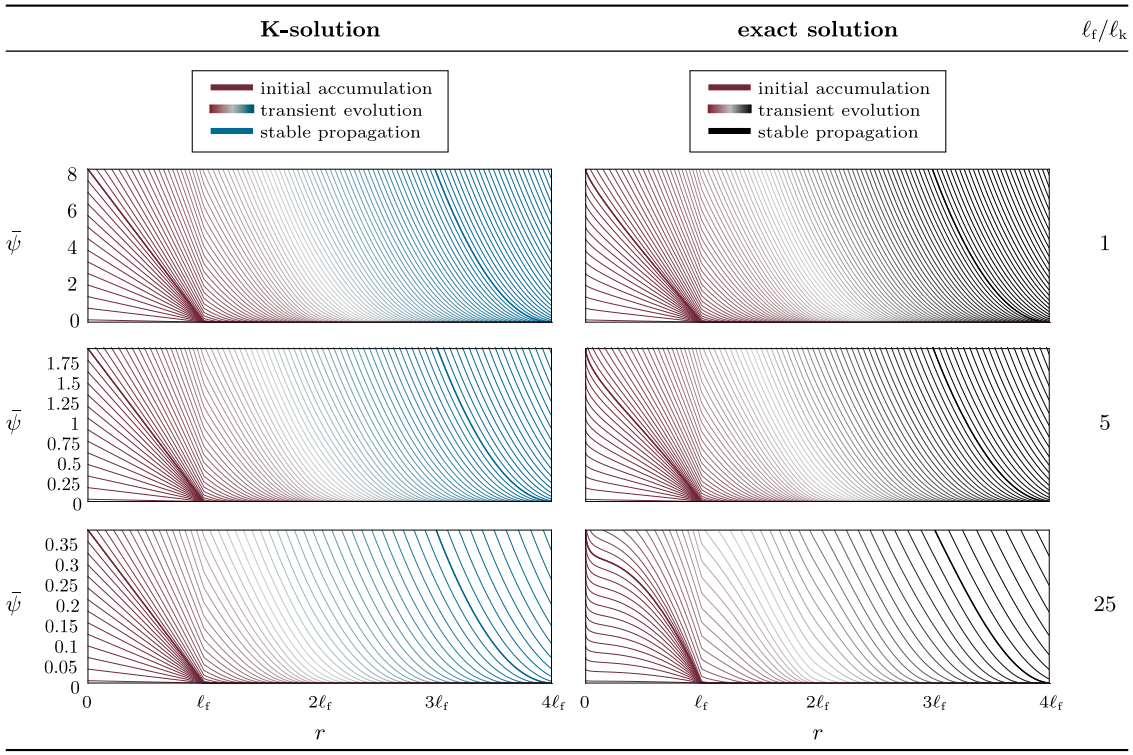

(a) Analyses with the linear threshold function h_l defined in (33).

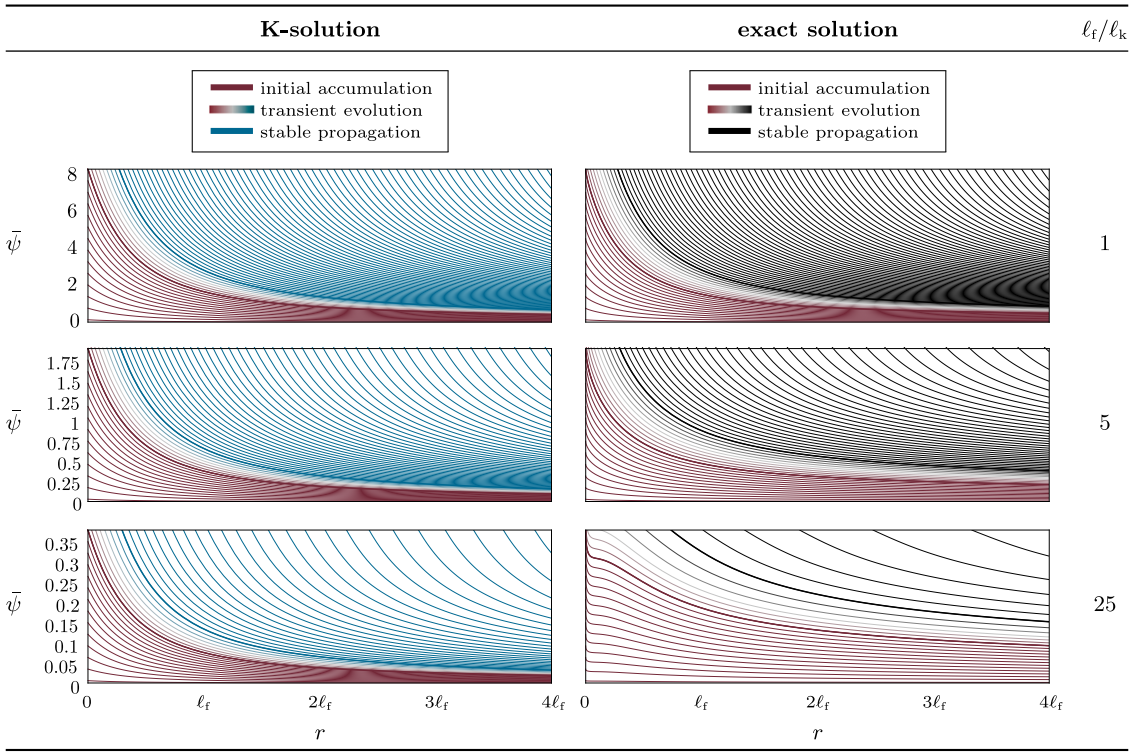

(b) Analyses with the exponential threshold function h_e defined in (34).

Fig. 21. Fatigue history variable profiles plotted every 5 load cycles for different values of ℓ_f/ℓ_k and for different threshold functions: (a) linear and (b) exponential. The transient evolution stage is only qualitatively identified.

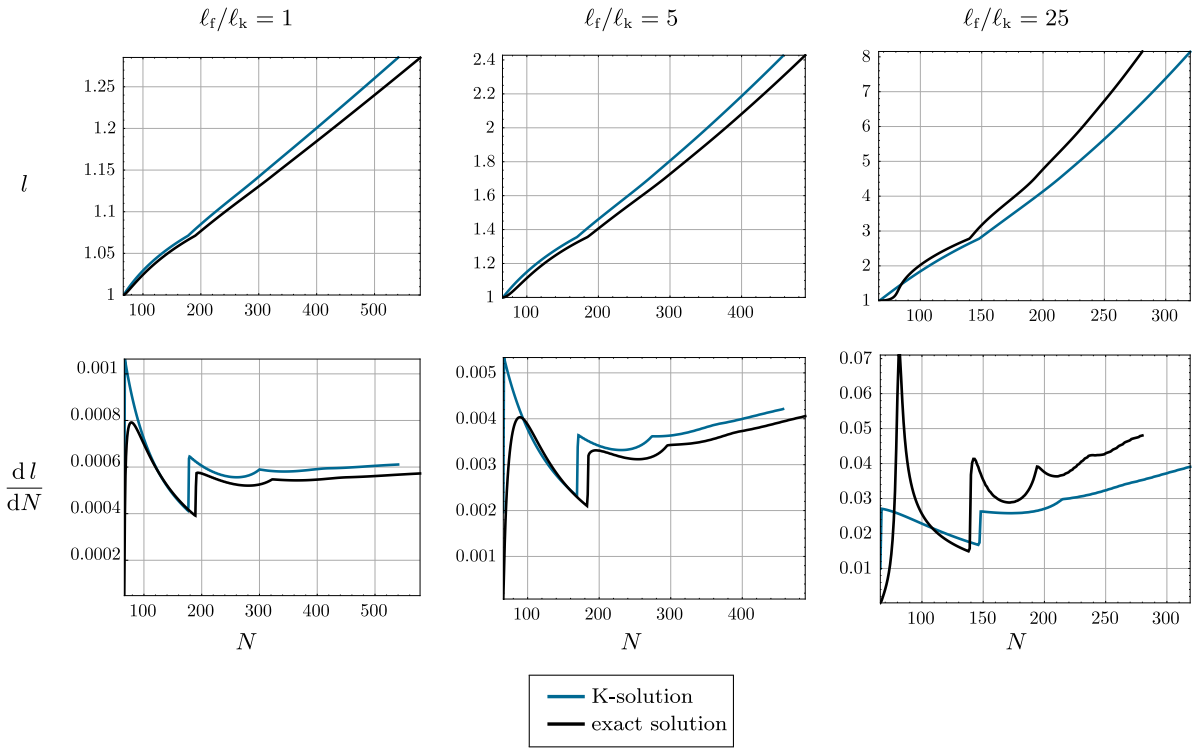

Fig. 22. Crack and crack rate evolutions with respect to the number of cycles for different values of ℓ_f/ℓ_k and for the linear threshold function h_l.

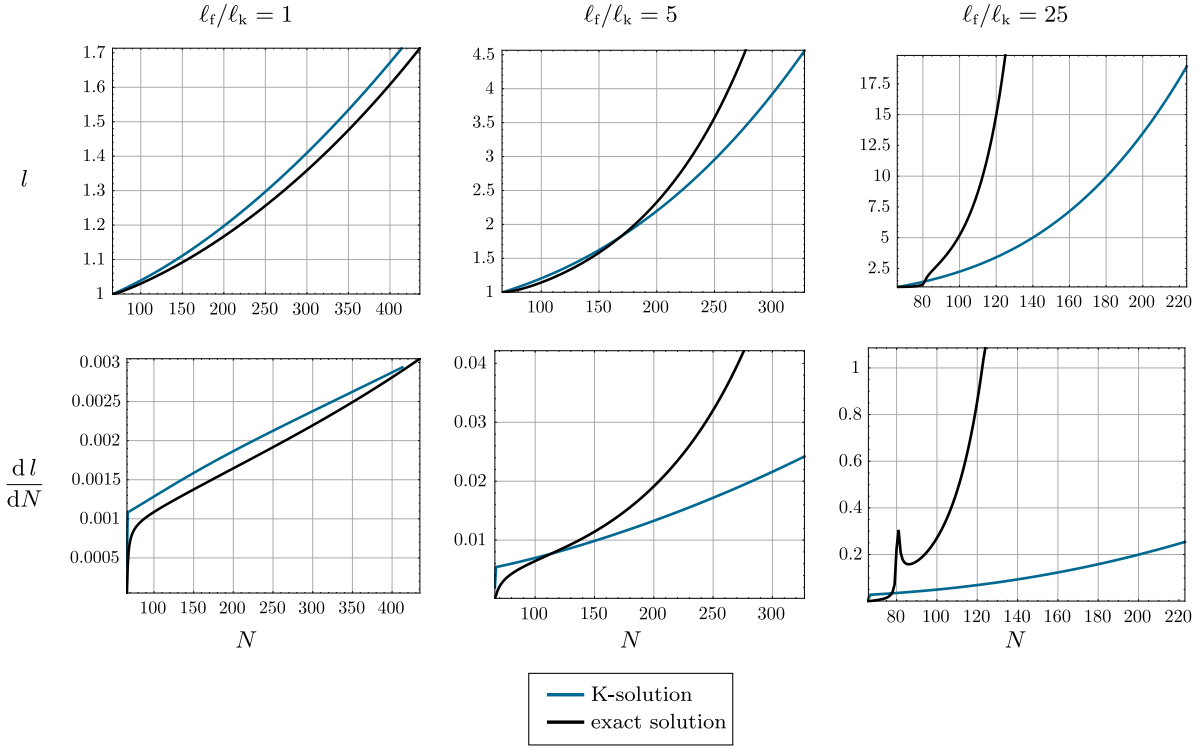

Fig. 23. Crack and crack rate evolutions with respect to the number of cycles for different values of ℓ_f/ℓ_k and for the exponential threshold function h_e.

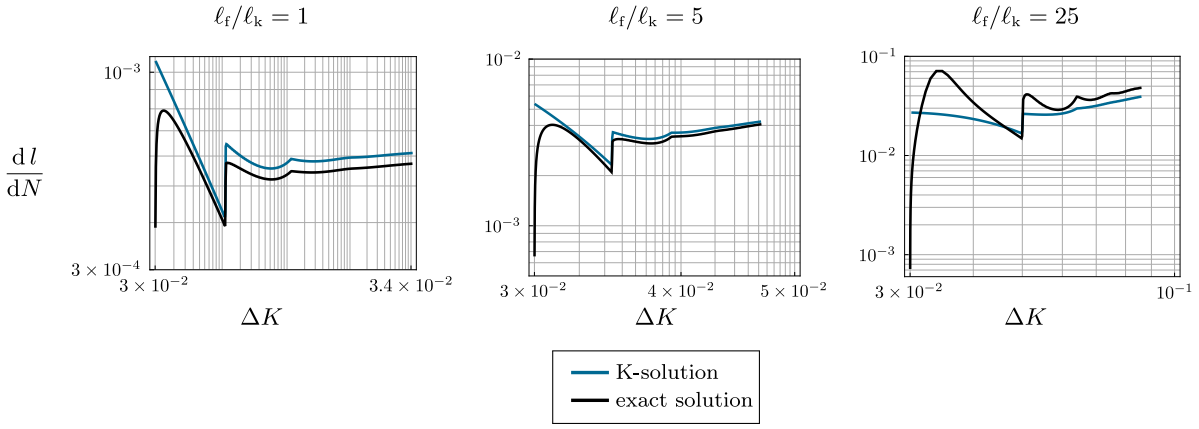

Fig. 24. Crack rate evolutions with respect to the stress intensity factor variation for different values of ℓ_f/ℓ_k and for the linear threshold function h_l.

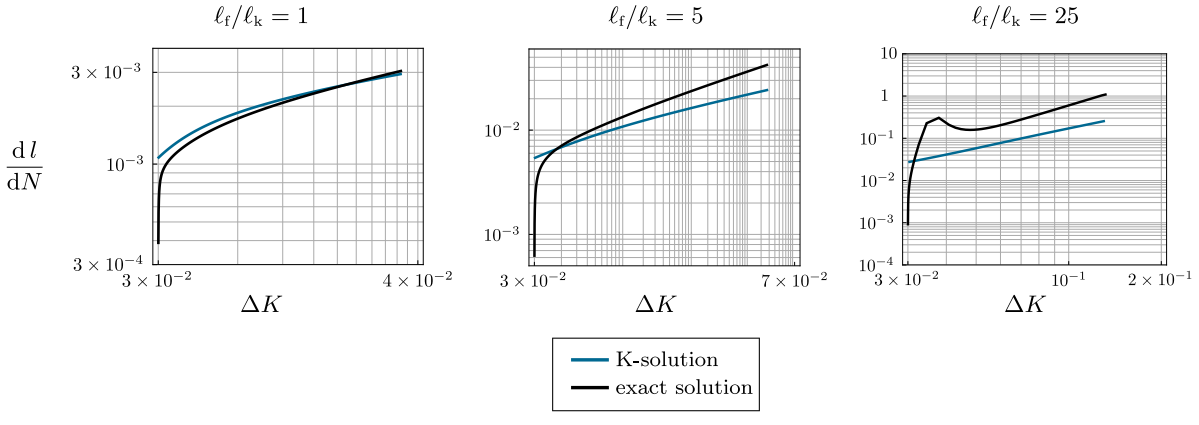

Fig. 25. Crack rate evolutions with respect to the stress intensity factor variation for different values of ℓ_f/ℓ_k and for the exponential threshold function h_e.

the exponential threshold function, one can observe an increment of the fatigue history variable, and therefore a material fatigue degradation, in the entire domain of analysis.

Concerning the crack and crack rate evolution with respect to the number of cycles, the K-solution and the exact solution provide quite similar results with the linear threshold function and for all considered length ratios. This behavior is also confirmed by Fig. 24, where the crack rate is plotted against the stress intensity factor variation. Instead, with the exponential threshold function, one can notice a progressive increment of the crack propagation rate with respect to the length ratio by considering the exact solution instead of the K-solution. This difference is quite noticeable in Fig. 23 but less in the curves represented in the bi-logarithmic scale in Fig. 25. Summing up, we can conclude that if the linear threshold function is adopted, the difference in the fatigue crack propagation behavior resulting from the K-solution and the exact solution is small whereas it is much larger if h_e is considered. This is due to the fact that h_e accounts for energy contributions far from the crack tip, where the energetic contribution of the exact solution to the fatigue history variable is relevant, while the contribution deriving from the K-solution is negligible (Fig. 20).

It is worth noticing from Fig. 25 that models based on the exponential threshold function seem to be able to better describe the slow fatigue crack initiation, as occurring in SR, with respect to the linear threshold model. The reason lies in the fact that the resulting fatigue history variable profile at incipient propagation, with respect to the profile in the PR, is smaller with h_e but larger with h_l.

4. Conclusions

In this work, an extension of Griffith's fracture theory to describe fatigue-induced fracture has been proposed. This task was achieved by introducing a state-dependent fracture toughness, degraded in terms of a fatigue history variable. The proposed modeling approach encompasses complex fatigue processes in a simple yet flexible form while preserving a direct link with classical fracture mechanics. Specifically, a composition of constitutive functions was introduced to define an energy-based fatigue history variable. Each of these functions considers one of the following mechanisms: (i) the crack tip singularity, (ii) the identification of fatigue-inducing loading conditions, (iii) mean stress effects, and (iv) the effect of consecutive loading. This last aspect has been proven to be the key for tuning Paris' law exponent during stationary fatigue crack propagation.

To address the capabilities of the model, a simple 2D benchmark example, for which the exact analytical solution is available in the framework of linear elastic fracture mechanics, was studied in depth. The results of this study revealed different consecutive processes involved in fatigue crack propagation, namely, an initial accumulation, a transient stage, and a stable propagation stage. In addition, compact analytical results showed that already simple forms of the model recover the celebrated Paris' law as well Forman's extension to mean stress effects and the fast propagation stage. However, in the present model, the parameters are easily tuned and are directly related to Griffith's fracture theory. To the authors' knowledge, previous studies have not been able to provide such a link. Finally, the size of the fatigue zone relative to the K-dominance zone was addressed in the context of alternative forms of the model. It was shown that far field effects, which may be taken into account by the model, may play a significant role in cases where the fatigue degradation zone contains the K-dominance zone.

The developments presented in this first study allow us to envisage a new generation of numerical models to describe fatigue processes in different materials. In particular, the phase-field fracture models with fatigue effects, presented in a persistently growing body of literature, share a common shortcoming: a missing link with a physical Griffith-based fracture theory. The present study provides a framework to overcome this shortcoming and may be taken as the point of departure to develop a consistent phase-field model for fatigue-induced fracture. Furthermore, it could be interesting to extend the model, exploiting its intrinsic flexibility, to consider non-proportional loading conditions [3], inelastic phenomena [17], undefined crack paths [77], mixed-fracture modes [78], and related numerical issues [79].

CRediT authorship contribution statement

Roberto Alessi: Writing – review & editing, Writing – original draft, Methodology, Formal analysis, Conceptualization. **Jacinto Ulloa:** Writing – review & editing, Writing – original draft, Methodology, Formal analysis, Conceptualization.

Declaration of competing interest

The authors declare that they have no known competing financial interests or personal relationships that could have appeared to influence the work reported in this paper.

Data availability

No data was used for the research described in the article.

Acknowledgments

Roberto Alessi wishes to acknowledge the support of: the Italian National Group of Mathematical Physics INdAM-GNFM; the University of Pisa through the project PRA 2022 69 "Advanced modelling of ultra-lightweight materials and structures"; the Project PRIN 2017 20177TTP3S; the program FSE REACT EU-PONRI 2014–2020. Roberto Alessi is also thankful to Prof. Giovanni Lancioni for insightful discussions on the topic.

Appendix. Mode-I fracture in an infinite two-dimensional domain

In this section, we recall the expressions for the stress and energy fields of an infinite plane with a symmetric crack (IPSC) of length $2l$ subjected to a uniaxial stress σ at infinity. This setup is one of the most typical crack problems in fracture mechanics for which the exact solution is available. Thus, in this case, it is possible to compare the exact solution with the near-tip K-stress solution.

The problem is highlighted in Fig. A.26. According to the chosen reference system, the boundary conditions read

$$\begin{cases} \sigma_{xy} = \sigma_{yy} = 0 & \text{at } |x| \leq l \text{ and } y = 0, \\ \sigma_{xx} = \sigma_{xy} = 0,\ \sigma_{yy} = \sigma & \text{at } x^2 + y^2 \to \infty. \end{cases} \tag{A.1}$$

The solution follows from the Westergaard function method within the complex potential approach for plane elasticity (Kolosov and Muskhelishvili formulas), as presented for instance in [38, Sec. 3]. The notation of this reference is adopted below.

Within this framework, the Westergaard function and constant for mode-I fracture read

$$Z_{\mathrm{I}}(z) = \frac{z}{\sqrt{z^2 - l^2}}\sigma \quad \text{and} \quad A = -\frac{\sigma}{2}, \tag{A.2}$$

with $z = r\,e^{i\vartheta}$ expressed in terms of polar coordinates in the complex plane. The constant A is related to the uniform uniaxial stress by the relation $\sigma_{xx} = 2A$. The associated stress component fields, as part of the *exact solution*, read

$$\begin{aligned} \sigma_{xx} &= \Re\left(Z_{\mathrm{I}}\right) - y\mathcal{I}\left(Z_{\mathrm{I}}'\right) + A \\ &= \frac{\sigma r}{\sqrt{r_1 r_2}}\left(\cos\left(\vartheta - \tfrac{1}{2}\vartheta_1 - \tfrac{1}{2}\vartheta_2\right) - \frac{l^2}{r_1 r_2}\sin\vartheta\sin\left(\tfrac{3}{2}\left(\vartheta_1 + \vartheta_2\right)\right)\right), \end{aligned} \tag{A.3a}$$

$$\begin{aligned} \sigma_{yy} &= \Re\left(Z_{\mathrm{I}}\right) + y\mathcal{I}\left(Z_{\mathrm{I}}'\right) \\ &= \frac{\sigma r}{\sqrt{r_1 r_2}}\left(\cos\left(\vartheta - \tfrac{1}{2}\vartheta_1 - \tfrac{1}{2}\vartheta_2\right) + \frac{l^2}{r_1 r_2}\sin\vartheta\sin\left(\tfrac{3}{2}\left(\vartheta_1 + \vartheta_2\right)\right)\right), \end{aligned} \tag{A.3b}$$

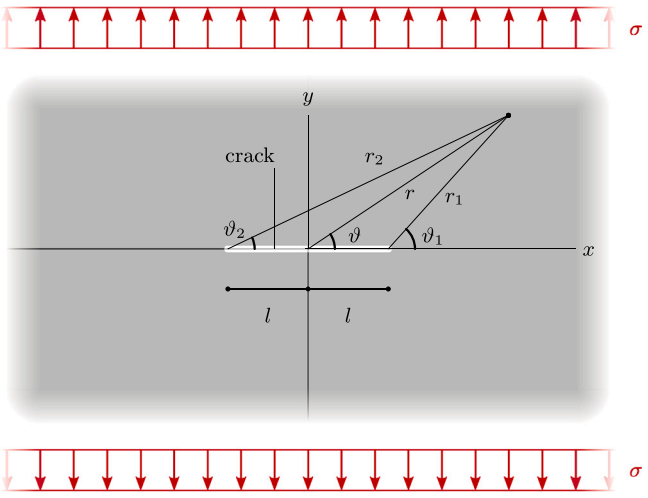

Fig. A.26. IPSC problem, reference system and variables.

$$\begin{aligned}\sigma_{xy} &= -y\Re\left(Z_{\mathrm{I}}'\right)\\ &= \frac{\sigma r}{\sqrt{r_1 r_2}}\left(\frac{l^2}{r_1 r_2}\sin\vartheta\cos\left(\tfrac{3}{2}\left(\vartheta_1+\vartheta_2\right)\right)\right),\end{aligned} \tag{A.3c}$$

with (r_1, ϑ_1) and (r_2, ϑ_2) clearly linked to (r, ϑ).

Instead, the *near-tip solution* or *approximated solution* with respect to the stress field reads

$$\tilde{\sigma}_{xx} = \frac{K_I}{\sqrt{2\pi r}}\cos\left(\frac{1}{2}\vartheta\left(1-\sin\frac{1}{2}\vartheta\sin\frac{3}{2}\vartheta\right)\right), \tag{A.4a}$$

$$\tilde{\sigma}_{yy} = \frac{K_I}{\sqrt{2\pi r}}\cos\left(\frac{1}{2}\vartheta\left(1+\sin\frac{1}{2}\vartheta\sin\frac{3}{2}\vartheta\right)\right), \tag{A.4b}$$

$$\tilde{\sigma}_{xy} = \frac{K_I}{\sqrt{2\pi r}}\sin\frac{1}{2}\vartheta\cos\frac{1}{2}\vartheta\cos\frac{3}{2}\vartheta, \tag{A.4c}$$

with $(r, \vartheta) \to (r_1, \vartheta_1)$ and the mode-I stress intensity factor given by

$$K_{\mathrm{I}} := \lim_{r\to 0}\sqrt{2\pi r}\,\sigma_{yy}(\vartheta = 0) = \sigma\sqrt{l\pi}. \tag{A.5}$$

Eqs. (A.3) and (A.4) evaluated along the straight propagation crack path, that is, for $\vartheta = \vartheta_1 = \vartheta_2 = 0$, $r = r_1 + l$, $r_2 = r_1 + 2l$, and $r_1 \to r$, become

$$\sigma_{xx} = \frac{\left(1+\frac{r}{l}\right)}{\sqrt{\pi l}\sqrt{2\frac{r}{l}+\left(\frac{r}{l}\right)^2}}K_{\mathrm{I}} - \sigma, \tag{A.6a}$$

$$\sigma_{yy} = \frac{\left(1+\frac{r}{l}\right)}{\sqrt{\pi l}\sqrt{2\frac{r}{l}+\left(\frac{r}{l}\right)^2}}K_{\mathrm{I}}, \tag{A.6b}$$

$$\sigma_{xy} = 0, \tag{A.6c}$$

and

$$\tilde{\sigma}_{xx} = \frac{1}{\sqrt{2\pi r}}K_{\mathrm{I}}, \tag{A.7a}$$

$$\tilde{\sigma}_{yy} = \frac{1}{\sqrt{2\pi r}}K_{\mathrm{I}}, \tag{A.7b}$$

$$\tilde{\sigma}_{xy} = 0, \tag{A.7c}$$

respectively. These are displayed in Fig. A.27. A first difference between (A.3) and (A.4) or between (A.6) and (A.7) is that the exact solution explicitly depends on the actual crack extent whereas the approximated solution does not.

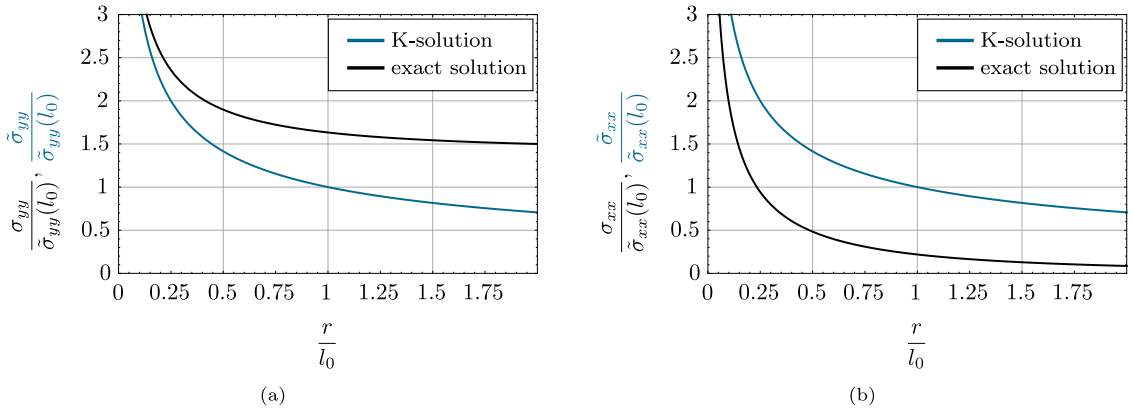

Fig. A.27. Stress profiles for the K-solution and the exact solution.

Accordingly, the exact elastic energy density takes, for a plane-stress problem, the following expression along the crack propagation path:

$$\psi = \frac{2K_{\mathrm{I}}^2(1-\nu)(1+\lambda)^2 - 2\sqrt{l}K_{\mathrm{I}}\sqrt{\pi}(1-\nu)(1+\lambda)\sqrt{\lambda(2+\lambda)}\sigma + l\pi\lambda(2+\lambda)\sigma^2}{2lE\pi\lambda(2+\lambda)}, \tag{A.8}$$

with $\lambda = r/l$. In contrast, the elastic energy density relying only on the approximated solution, that is, the K-stress solution, is given by

$$\psi_{\mathrm{K}}(r) = \frac{K_{\mathrm{I}}^2(1-\nu)}{2\pi\, E\, r}. \tag{A.9}$$

Plane-strain expressions can be obtained with the following straightforward substitutions: $E \to E/(1-\nu^2)$ and $\nu \to \nu/(1-\nu)$.

References

[1] Suresh S. Fatigue of Materials. Cambridge University Press; 1998, p. 679.
[2] Schijve J. Fatigue of Structures and Materials. Springer; 2009.
[3] Skibicki D. Phenomena and Computational Models of Non-Proportional Loadings. Springer International Publishing; 2014, p. 126.
[4] Stephens RRI, Fatemi A, Stephens RRI, Fuchs HO. Metal Fatigue in Engineering. A Wiley-Interscience publication, John Wiley & Sons; 2000, http://dx.doi.org/10.1115/1.3225026.
[5] Griffith AA. The phenomena of rupture and flow in solids. Philos Trans R Soc Lond 1921;A221:163–98, URL http://www.jstor.org/stable/91192.
[6] Francfort GA, Marigo J-J. Revisiting brittle fracture as an energy minimization problem. J Mech Phys Solids 1998;46(8):1319–42. http://dx.doi.org/10.1016/S0022-5096(98)00034-9, URL http://www.sciencedirect.com/science/article/B6TXB-3XDH3V4-2/2/6078bc5b38861a78a6b1044a60e0a4bb.
[7] Bourdin B, Francfort GA, Marigo J-J. Numerical experiments in revisited brittle fracture. J Mech Phys Solids 2000;48(4):797–826. http://dx.doi.org/10.1016/S0022-5096(99)00028-9, URL http://linkinghub.elsevier.com/retrieve/pii/S0022509699000289.
[8] Bourdin B, Francfort GA, Marigo J-J. The Variational Approach to Fracture. J Elasticity 2008;91(1):5–148. http://dx.doi.org/10.1007/s10659-007-9107-3, URL http://www.springerlink.com/content/31370771n83r2637.
[9] Schreiber C, Kuhn C, Müller R. On phase field modeling in the context of cyclic mechanical fatigue. Pamm 2019;19(1):2–3. http://dx.doi.org/10.1002/pamm.201900104.
[10] Schreiber C, Kuhn C, Müller R, Zohdi T. A phase field modeling approach of cyclic fatigue crack growth. Int J Fract 2020;225(1):89–100. http://dx.doi.org/10.1007/s10704-020-00468-w.
[11] Yan S, Schreiber C, Müller R. An efficient implementation of a phase field model for fatigue crack growth. Int J Fract 2022. http://dx.doi.org/10.1007/s10704-022-00628-0.
[12] Alessi R, Vidoli S, De Lorenzis L. A phenomenological approach to fatigue with a variational phase-field model: The one-dimensional case. Eng Fract Mech 2018;190:53–73. http://dx.doi.org/10.1016/j.engfracmech.2017.11.036.
[13] Alessi R. Energetic formulation for rate-independent processes: remarks on discontinuous evolutions with a simple example. Acta Mech 2016;227(10):2805–29. http://dx.doi.org/10.1007/s00707-016-1636-z, URL http://link.springer.com/article/10.1007/s00707-016-1636-z.
[14] Alessi R, Crismale V, Orlando G. Fatigue Effects in Elastic Materials with Variational Damage Models: A Vanishing Viscosity Approach. J Nonlinear Sci 2019;29(3). http://dx.doi.org/10.1007/s00332-018-9511-9.
[15] Carrara P, Ambati M, Alessi R, De Lorenzis L. A framework to model the fatigue behavior of brittle materials based on a variational phase-field approach. Comput Methods Appl Mech Engrg 2020;361:112731. http://dx.doi.org/10.1016/j.cma.2019.112731, URL http://www.sciencedirect.com/science/article/pii/S0045782519306218.
[16] Titscher T, Unger JF. Efficient higher-order cycle jump integration of a continuum fatigue damage model. Int J Fatigue 2020;141(August):105863. http://dx.doi.org/10.1016/j.ijfatigue.2020.105863.
[17] Ulloa J, Wambacq J, Alessi R, Degrande G, François S. Phase-field modeling of fatigue coupled to cyclic plasticity in an energetic formulation. Comput Methods Appl Mech Engrg 2021;373:113473. http://dx.doi.org/10.1016/j.cma.2020.113473, arXiv:1910.10007.
[18] Seleš K, Aldakheel F, Tonković Z, Sorić J, Wriggers P. A general phase-field model for fatigue failure in brittle and ductile solids. Comput Mech 2021;67(5):1431–52. http://dx.doi.org/10.1007/s00466-021-01996-5.
[19] Yin B, Kaliske M. A ductile phase-field model based on degrading the fracture toughness: Theory and implementation at small strain. Comput Methods Appl Mech Engrg 2020;366:113068. http://dx.doi.org/10.1016/j.cma.2020.113068.

[20] Ai W, Wu B, Martínez-Pañeda E. A coupled phase field formulation for modelling fatigue cracking in lithium-ion battery electrode particles. J Power Sources 2022;544:231805. http://dx.doi.org/10.1016/j.jpowsour.2022.231805, URL https://linkinghub.elsevier.com/retrieve/pii/S0378775322007959.

[21] Seiler M, Linse T, Hantschke P, Kästner M. An efficient phase-field model for fatigue fracture in ductile materials. Eng Fract Mech 2020;224:106807. http://dx.doi.org/10.1016/j.engfracmech.2019.106807, arXiv:1903.06465.

[22] Seiler M, Keller S, Kashaev N, Klusemann B, Kästner M. Phase-field modelling for fatigue crack growth under laser shock peening-induced residual stresses. Arch Appl Mech 2021;91(8):3709–23. http://dx.doi.org/10.1007/s00419-021-01897-2.

[23] Schneider T, Müller D, Seiler M, Tobie T, Stahl K, Kästner M. Phase-field modeling of fatigue crack growth during tooth flank fracture in case-hardened spur gears. Int J Fatigue 2022;163:107091. http://dx.doi.org/10.1016/j.ijfatigue.2022.107091, URL https://www.sciencedirect.com/science/article/pii/S0142112322003516.

[24] Yin B, Khodor J, Kaliske M. Fracture and Fatigue Failure Simulation of Polymeric Material at Finite Deformation by the Phase-Field Method and the Material Force Approach. Adv. Polym. Sci. 2021;286:347–76. http://dx.doi.org/10.1007/12_2020_63.

[25] Lo Y-S, Borden MJ, Ravi-Chandar K, Landis CM. A Phase-field Model for Fatigue Crack Growth. J Mech Phys Solids 2019;103684. http://dx.doi.org/10.1016/j.jmps.2019.103684.

[26] Amendola G, Fabrizio M, Golden JM. Thermomechanics of damage and fatigue by a phase field model. J. Therm. Stresses 2016;39(5):487–99. http://dx.doi.org/10.1080/01495739.2016.1152140, arXiv:1410.7042.

[27] Eleuteri M, Kopfová J, Krejčí P. A new phase field model for material fatigue in an oscillating elastoplastic beam. Discrete Contin Dyn Syst Ser A 2015;35(6):2465–95. http://dx.doi.org/10.3934/dcds.2015.35.2465.

[28] Boldrini JL, Barros de Moraes EA, Chiarelli LR, Fumes FG, Bittencourt ML. A non-isothermal thermodynamically consistent phase field framework for structural damage and fatigue. Comput Methods Appl Mech Engrg 2016. http://dx.doi.org/10.1016/j.cma.2016.08.030.

[29] Haveroth GA, Vale MG, Bittencourt ML, Boldrini JL. A non-isothermal thermodynamically consistent phase field model for damage, fracture and fatigue evolutions in elasto-plastic materials. Comput Methods Appl Mech Engrg 2020;364:112962. http://dx.doi.org/10.1016/j.cma.2020.112962.

[30] Loew PJ, Peters B, Beex LAA. Fatigue phase-field damage modeling of rubber. In: Constitutive Models for Rubber XI. 2019, p. 408–12. http://dx.doi.org/10.1201/9780429324710-72.

[31] Loew PJ, Poh LH, Peters B, Beex LAA. Accelerating fatigue simulations of a phase-field damage model for rubber. Comput Methods Appl Mech Engrg 2020;370:113247. http://dx.doi.org/10.1016/j.cma.2020.113247.

[32] Loew PJ, Peters B, Beex LA. Fatigue phase-field damage modeling of rubber using viscous dissipation: Crack nucleation and propagation. Mech Mater 2020;142(December 2019):103282. http://dx.doi.org/10.1016/j.mechmat.2019.103282.

[33] Tada H, Paris PC, Irwin GR. the Stress Analysis of Cracks Handbook. 2000.

[34] Ostash OP, Panasyuk VV. Fatigue process zone at notches. Int J Fatigue 2001;23(7):627–36. http://dx.doi.org/10.1016/S0142-1123(01)00004-4.

[35] Ostash OP, Panasyuk VV, Kostyk EM. A phenomenological model of fatigue macrocrack initiation near stress concentrators. Fatigue Fract Eng Mater Struct 1999;22(2):161–72. http://dx.doi.org/10.1046/j.1460-2695.1999.00098.x, URL https://onlinelibrary.wiley.com/doi/abs/10.1046/j.1460-2695.1999.00098.x.

[36] Grossman-Ponemon BE, Mesgarnejad A, Karma A. Phase-field modeling of continuous fatigue via toughness degradation. Eng Fract Mech 2022;264(November 2021):108255. http://dx.doi.org/10.1016/j.engfracmech.2022.108255.

[37] Halphen B, Nguyen QS. Generalized Standard Materials. J.e Méc. 1975;14(1):39–63.

[38] Sun CT, Jin Z. Fracture Mechanics. Elsevier Science; 2012, URL https://books.google.it/books?id=LfqMaqVw-jMC.

[39] Gross D, Seelig T. Fracture Mechanics: With an Introduction to Micromechanics. Mechanical Engineering Series, Springer Berlin Heidelberg; 2006, URL https://books.google.it/books?id=xuby9HLd8GAC.

[40] Almi S, Lucardesi I. Energy release rate and stress intensity factors in planar elasticity in presence of smooth cracks. Nonlinear Differ. Equ. Appl. 2018;25(5):1–28. http://dx.doi.org/10.1007/s00030-018-0536-4.

[41] Sun CT, Qian H. Brittle fracture beyond the stress intensity factor. J Mech Mater Struct 2009;4(4):743–53. http://dx.doi.org/10.2140/jomms.2009.4.743.

[42] Kumar B, Chitsiriphanit S, Sun CT. Significance of K-dominance zone size and nonsingular stress field in brittle fracture. Eng Fract Mech 2011;78(9):2042–51. http://dx.doi.org/10.1016/j.engfracmech.2011.03.015.

[43] Pook LP. The effect of crack angle on fracture toughness. Eng Fract Mech 1971;3(3):205–18. http://dx.doi.org/10.1016/0013-7944(71)90032-4.

[44] Shen B, Stephansson O. Modification of the G-criterion for crack propagation subjected to compression. Eng Fract Mech 1994;47(2):177–89. http://dx.doi.org/10.1016/0013-7944(94)90219-4, URL https://linkinghub.elsevier.com/retrieve/pii/0013794494902194.

[45] Gent AN. Engineering with Rubber: How to Design Rubber Components. third ed.. Hanser Publishers, Carl Hanser Verlag GmbH & Co; 2012, http://dx.doi.org/10.5254/1.3538214, URL.

[46] Dammaß F, Kalina KA, Ambati M, Kästner M. Phase-field modelling and analysis of rate-dependent fracture phenomena at finite deformation. 2022, p. 1–22, arXiv:2206.03460.

[47] Jiang D, Carter EA. First principles assessment of ideal fracture energies of materials with mobile impurities: implications for hydrogen embrittlement of metals. Acta Mater 2004;52(16):4801–7. http://dx.doi.org/10.1016/j.actamat.2004.06.037, URL https://linkinghub.elsevier.com/retrieve/pii/S1359645404003854.

[48] Wang Y, Gong J, Jiang W. A quantitative description on fracture toughness of steels in hydrogen gas. Int J Hydrogen Energy 2013;38(28):12503–8. http://dx.doi.org/10.1016/j.ijhydene.2013.07.033.

[49] Martínez-Pañeda E, Golahmar A, Niordson CF. A phase field formulation for hydrogen assisted cracking. Comput Methods Appl Mech Engrg 2018;342:742–61. http://dx.doi.org/10.1016/j.cma.2018.07.021, arXiv:1808.03264.

[50] Hirshikesh, Natarajan S, Annabattula RK, Martínez-Pañeda E. Phase field modelling of crack propagation in functionally graded materials. Composites B 2019;169:239–48. http://dx.doi.org/10.1016/j.compositesb.2019.04.003, URL https://linkinghub.elsevier.com/retrieve/pii/S135983681930229X.

[51] Dsouza SM, Hirshikesh, Mathew TV, Singh IV, Natarajan S. A non-intrusive stochastic phase field method for crack propagation in functionally graded materials. Acta Mech 2021;232(7):2555–74. http://dx.doi.org/10.1007/s00707-021-02956-z.

[52] Lancioni G, Alessi R. Modeling micro-cracking and failure in short fiber-reinforced composites. J Mech Phys Solids 2020;137:103854. http://dx.doi.org/10.1016/j.jmps.2019.103854.

[53] Zehnder AT. Fracture Mechanics. Springer Verlag; 2012, http://dx.doi.org/10.1007/978-3-642-33968-4.

[54] Aliha MR, Ayatollahi MR. Geometry effects on fracture behaviour of polymethyl methacrylate. Mater Sci Eng A 2010;527(3):526–30. http://dx.doi.org/10.1016/j.msea.2009.08.055.

[55] Tutluoglu L, Keles C. Effects of geometric factors on mode I fracture toughness for modified ring tests. Int J Rock Mech Min Sci 2012;51:149–61. http://dx.doi.org/10.1016/j.ijrmms.2012.02.004.

[56] Paris P, Erdogan F. A critical analysis of crack propagation laws. J. Fluids Eng. Trans. ASME 1963;85(4):528–33. http://dx.doi.org/10.1115/1.3656900.

[57] Paris PC, Gomez MP, Anderson WEP. A Rational Analytic Theory of Fatigue. In: The Trend in Engineering, vol. 13. 1961, p. 9–14.

[58] Forman RG, Kearney VE, Engle RM. Numerical analysis of crack propagation in cyclic-loaded structures. J. Fluids Eng. Trans. ASME 1967;89(3):459–63. http://dx.doi.org/10.1115/1.3609637.

[59] Priddle EK. High cycle fatigue crack propagation under random and constant amplitude loadings. Int J Press Vessels Pip 1976;4:89.

[60] Klesnil M, Lukáš P. Influence of strength and stress history on growth and stabilisation of fatigue cracks. Eng Fract Mech 1972;4(1):77–92. http://dx.doi.org/10.1016/0013-7944(72)90078-1.

[61] Mettu S, Shivakumar V, Beek J, Yeh F, Williams L, Forman R, McMahon J, Newman I. NASGRO 3.0: A software for analyzing aging aircraft. Technical Report, 1999, URL https://www.researchgate.net/publication/4687258_NASGRO_30_A_software_for_analyzing_aging_aircraft.
[62] Klysz S, Leski A. Good Practice for Fatigue Crack Growth Curves Description. Appl. Fracture Mech. 2012;(October). http://dx.doi.org/10.5772/52794.
[63] Elber W. Fatigue crack closure under cyclic tension. Eng Fract Mech 1970;2(1):37–44. http://dx.doi.org/10.1016/0013-7944(70)90028-7.
[64] Rabold F, Kuna M. Automated Finite Element Simulation of Fatigue Crack Growth in Three-dimensional Structures with the Software System ProCrack. Procedia Mater. Sci. 2014;3:1099–104. http://dx.doi.org/10.1016/j.mspro.2014.06.179.
[65] Rabold F, Kuna M, Leibelt T. Procrack: A Software for Simulating Three-Dimensional Fatigue Crack Growth. In: Apel T, Steinbach O, editors. Advanced Finite Element Methods and Applications. Berlin, Heidelberg: Springer Berlin Heidelberg; 2013, p. 355–74. http://dx.doi.org/10.1007/978-3-642-30316-6_16.
[66] Qian J, Fatemi A. Mixed mode fatigue crack growth: A literature survey. Eng Fract Mech 1996;55(6):969–90. http://dx.doi.org/10.1016/S0013-7944(96)00071-9.
[67] Gdoutos EE, Rodopoulos CA, Yates JR. Problems of Fracture Mechanics and Fatigue: A Solution Guide. 2003.
[68] Blaiszik BJ, Kramer SL, Olugebefola SC, Moore JS, Sottos NR, White SR. Self-healing polymers and composites. Annu Rev Mater Res 2010;40:179–211. http://dx.doi.org/10.1146/annurev-matsci-070909-104532.
[69] Ulloa J, Alessi R, Wambacq J, Degrande G, François S. On the variational modeling of non-associative plasticity. Int J Solids Struct 2021;217–218.
[70] Sih GC. Strain-energy-density factor applied to mixed mode crack problems. Int J Fract 1974;10(3):305–21. http://dx.doi.org/10.1007/BF00035493, URL http://link.springer.com/10.1007/BF00035493.
[71] Mesgarnejad A, Imanian A, Karma A. Phase-field models for fatigue crack growth. Theor Appl Fract Mech 2019;103(December 2018):102282. http://dx.doi.org/10.1016/j.tafmec.2019.102282.
[72] Köbler J, Magino N, Andrä H, Welschinger F, Müller R, Schneider M. A computational multi-scale model for the stiffness degradation of short-fiber reinforced plastics subjected to fatigue loading. Comput Methods Appl Mech Engrg 2021;373:113522. http://dx.doi.org/10.1016/j.cma.2020.113522.
[73] Miehe C, Hofacker M, Welschinger FR. A phase field model for rate-independent crack propagation: Robust algorithmic implementation based on operator splits. Comput Methods Appl Mech Engrg 2010;199(45–48):2765–78. http://dx.doi.org/10.1016/j.cma.2010.04.011, URL http://linkinghub.elsevier.com/retrieve/pii/S0045782510001283.
[74] Hasan MM, Baxevanis T. A phase-field model for low-cycle fatigue of brittle materials. Int J Fatigue 2021;150(January):106297. http://dx.doi.org/10.1016/j.ijfatigue.2021.106297.
[75] Simoes M, Martínez-Pañeda E. Phase field modelling of fracture and fatigue in Shape Memory Alloys. Comput Methods Appl Mech Engrg 2021;373:113504. http://dx.doi.org/10.1016/j.cma.2020.113504, arXiv:2010.04390.
[76] Irwin GR. Analysis of Stresses and Strains Near the End of a Crack Traversing a Plate. J Appl Mech 1957.
[77] Crismale V, Lazzaroni G. Quasistatic crack growth based on viscous approximation: a model with branching and kinking. NoDEA Nonlinear Differential Equations Appl 2017;24(1):7. http://dx.doi.org/10.1007/s00030-016-0426-6, URL https://link.springer.com/10.1007/s00030-016-0426-6.
[78] De Lorenzis L, Maurini C. Nucleation under multi-axial loading in variational phase-field models of brittle fracture. Int J Fract 2021. http://dx.doi.org/10.1007/s10704-021-00555-6, URL https://link.springer.com/10.1007/s10704-021-00555-6.
[79] Freddi F, Mingazzi L. Mesh refinement procedures for the phase field approach to brittle fracture. Comput Methods Appl Mech Engrg 2022;388:114214. http://dx.doi.org/10.1016/j.cma.2021.114214, URL https://linkinghub.elsevier.com/retrieve/pii/S0045782521005454.